

**Supplementary Materials for
Expansion of a bacterial operon during cancer treatment ameliorates fluoropyrimidine
toxicity**

This file includes:

Supplementary Materials and Methods
Figs. S1-S17
Tables S1-S3
References (73-90)

Other Supplementary Material for this manuscript includes:

Data Files S1-S8
MDAR Reproducibility Checklist

MATERIALS AND METHODS

Clinical study design

The Gut microbiome and Oral fluoropyrimidine (GO) study was an observational clinical study registered at ClinicalTrials.gov under the identifier NCT04054908. All participants provided informed consent. The study was approved by the UCSF Institutional Review Board. Participants were recruited and sampled, without any compensation, at UCSF from the study start date (2018/04/13) to end date (2022/06/30). Inclusion criteria included: 18 years or older, histologically confirmed colorectal adenocarcinoma, and expected to receive oral fluoropyrimidine therapy. Patients who met any of the following criteria were excluded: known HIV positive diagnosis, chemotherapy, biologic or immunotherapy in the previous 2 weeks, exposure to ≥ 2 weeks antibiotics in the last 6 months, or exposure to antibiotics in the past 4 weeks. Patients were enrolled to one of three subcohorts: subcohort A received oral CAP as part of standard-of-care therapy; subcohort B received TAS-102 (trifluridine/tipiracil) \pm Y-90 radioembolization (73); subcohort C received CAP + α -PD1 immunotherapy (pembrolizumab) + bevacizumab as part of a separate clinical trial (NCT03396926). Patients with concurrent rectal radiation therapy (RT) were originally excluded, but the eligibility criteria were amended to include patients with concurrent rectal RT to increase enrollment. CAP and TAS-102 tablets were prescribed according to FDA labels for oral dosing. CAP tablets were taken twice daily on days 1–14 of a 21-day Cycle (no RT) or on days of radiation only (RT); TAS-102 tablets were taken twice daily on days 1–5 and 8–12 of a 28-day Cycle. Stool collection occurred at home before chemotherapy initiation and on day 1 of Cycles 1, 2, 3. During Cycle 1, stool was also collected at day 3 and midpoint (day 7 for subcohorts A, C; day 10 for subcohort B). Actual collection days are plotted in fig. S1. Stool samples were collected on fecal occult blood test (FOBT) cards for all time points. Additional bulk scoop samples were collected at baseline for culturing. Stool was stored at -80°C upon receipt at UCSF. 222 stool samples from 40 participants on FOBT cards were ultimately evaluable; 4 samples were not evaluable due to insufficient extracted DNA quantity. Methods for longitudinal sampling of small intestinal contents were not widely available at the time of GO study initiation (April 13th, 2018).

Resources Table

Reagent	Source	Catalog Number
Capecitabine	Fisher Scientific	50148375
Capecitabine- $^{2}\text{H}_{11}$	Santa Cruz Biotechnology	1132662
5-fluorouracil	Millipore Sigma	F6627
5-fluorouracil- $^{13}\text{C}, ^{15}\text{N}_2$	Santa Cruz Biotechnology	217189
Citric acid	Thomas Scientific	C752W30
Sodium citrate dihydrate	Fisher Scientific	18613454

Gum arabic	Spectrum Chemicals	GU113
<i>Escherichia coli</i> Δ <i>preTA</i>	(15)	N/A
<i>Escherichia coli</i> <i>preTA-wt</i>	(15)	N/A
<i>Escherichia coli</i> <i>preTA</i> ⁺⁺	(15)	N/A
Bacto Brain Heart Infusion (broth)	Fisher Scientific	237500
L-Cysteine HCl	Fisher Scientific	C81020
Hemin	Fisher Scientific	51280
Menadione (Vitamin K)	Fisher Scientific	102259
Lysogeny broth (LB)	Millipore Sigma	L3152
Eosin Methylene Blue (EMB) agar	Thomas Scientific	C5701
Streptomycin	Thomas Scientific	S6501
Neomycin	Neta Scientific	SIAL-N1876
Azithromycin	Neta Scientific	FISHUCOP-A20765G
Vancomycin	Thomas Scientific	C752X68
Metronidazole	Neta Scientific	SIAL-M1547-25G
Sucrose	Thomas Scientific	C752W82
Dimethyl sulfoxide	Millipore Sigma	D8418
Mouse Lipocalin-2/NGAL DuoSet ELISA	Fisher Scientific	DY185705
ZymoBIOMICS 96 MagBead DNA Kit	Zymo Research	D4302
SYBR Green I	Millipore Sigma	S9430
Nuclease-free water	Life Tech	0977-023
Phusion High-Fidelity PCR Kit	Thermo Scientific	F553L
QIAquick Gel Extraction Kit	Qiagen	28604
KAPA Library Quantification Kit	Roche	KK4824
MiSeq Reagent Kit v3 (600 cycles)	Illumina	MS-102-3003
Illumina DNA Prep, (M) Tagmentation (96 Samples, IPB)	Illumina	20060059
Quant-iT Picogreen dsDNA Kit	Invitrogen	P7589

SYBR Select	Life Technologies	4472908
Wildtype C57BL/6J mice	Jackson Labs	000664
Standard chow diet (SPF)	LabDiet	5058
Standard autoclaved chow diet	LabDiet	5021
BreatheEasy Covers	Millipore Sigma	Z380059

DNA extraction

ZymoBIOMICS 96 MagBead DNA Kit was used for DNA extractions. 750 µL of lysis solution was added to fecal aliquots (20–50 mg) in lysis tubes, while cell pellets from ex vivo communities were resuspended in 200 µL lysis solution and transferred to lysis tubes containing 550 µL lysis solution for a final volume of 750 µL lysis solution. Samples were homogenized with 5 min bead beating (Mini-Beadbeater-96, BioSpec), followed by 5 min room temperature (RT) incubation, and repeat 5 min bead beating. Samples were centrifuged for 1 min at 15,000 rcf, with 200 µL supernatant transferred into 1 mL deep-well plates and purified according to the manufacturer's instructions.

16S rRNA gene sequencing

The V4 region of the 16S rRNA gene was amplified using primers targeting 515F/806R regions (table S3). The reaction mix was 0.45 µL DMSO, 0.0045 µL SYBR Green I 10x diluted in DMSO to 1,000x, KAPA HiFi PCR kit (1.8 µL 5x KAPA HiFi Buffer, 0.27 µL 10 mM dNTPs, 0.18 µL KAPA HiFi polymerase), 0.045 µL of each amplification primer (final concentration 1 µM), 6.2055 µL nuclease-free water, and 1 µL DNA. A BioRad CFX 384 real-time PCR instrument amplified four 10-fold serial dilutions of DNA with the following parameters: 5 min 95°C, 20 x (20 sec 98°C, 15 sec 55°C, 60 sec 72°C), hold 4°C. Non-plateaued individual sample dilutions were selected for indexing PCR. KAPA HiFi PCR kit was used with 4 µL 5x KAPA HiFi Buffer, 0.6 µL 10 mM dNTPs, 1 µL DMSO, 0.4 µL KAPA HiFi polymerase, 4 µL indexing primer, 10 µL of 100-fold diluted primary PCR reaction. Secondary PCR amplification parameters were identical to Primary PCR. Amplicons were quantified with PicoGreen according to manufacturer's instructions, equimolar pooled, and gel purified (QIAquick Gel Extraction Kit). Libraries were quantified with KAPA Library Quantification Kit for Illumina Platforms according to the manufacturer's instructions, spiked with 15% PhiX, and sequenced on an Illumina MiSeqV3 instrument. Primers and adapters were removed using the cutadapt trim-paired command in QIIME2 (v2020.11) (58). Sequences underwent trimming to 220 bp (forward) or 150 bp (reverse), quality filtering, denoising, and chimera filtering using dada2 (v1.18.0) with QIIME2 command denoise-paired (74). Sequence length was filtered to 250–255 bp with QIIME2 command feature-table filter-seqs. Taxonomy was assigned to amplicon sequence variants (ASVs) using the SILVA v138 database (59). Sequence variants present in < 3 samples with ≥ 10 reads were removed from downstream analysis.

16S rRNA gene analysis

Alpha diversity metrics were computed with Phyloseq command estimate_richness (65). Differential alpha diversity was calculated with mixed effects model diversity ~ day + 1 | patient with the nlme (v3.1-164) command lme. ASV relative abundances were central log ratio (CLR)-transformed prior to further analysis. Principal coordinate analysis (PCoA) was performed with command prcomp (CLR-Euclidean ordination). PERMANOVA was performed using vegan (v2.6-4) commands vegdist (CLR-Euclidean ordination) and adonis2 (66), with Patient as a strata. Differential abundance was calculated using mixed effects model abundance ~ day + 1 | patient, followed by false discovery rate (FDR) correction with R command p.adjust, with FDR < 0.2 called as significant. ASV phylogenetic tree construction was performed with QIIME2 command phylogeny align-to-tree-mafft-fasttree. Line plots were plotted using ggplot2 (v3.5.1) command geom_smooth with LOESS regression (70). For comparisons of patient sensitivity with in vitro sensitivity, strain minimum inhibitory concentrations (MICs) were taken from (15).

Metagenomic sequencing

Shotgun libraries were prepared using the Illumina DNA Prep Tagationtation kit according to the manufacturer protocol. Libraries were assessed with PicoGreen and TapeStation 4200 (Agilent) for quantity and quality checks. Paired end libraries were sequenced using S1 flow cells on Illumina NovaSeq 6000 platforms. Demultiplexed reads underwent adapter trimming and quality filtering with FastP (v0.23.2) (60) and host read removal by mapping to human genome (GRCh38) with BMTagger (v3.101) (61). Genome equivalents were quantified with microbeCensus (v1.1.1) (64). Taxonomy was annotated with MetaPhlAn 4 (62). Genes were annotated with HUMAnN 3.0 (63), with UniRef90 families further mapped to KEGG Ortholog and Enzyme Class.

Metagenomic analysis

Gene abundances were normalized to reads per kilobase per genome equivalent (RPKG) using microbeCensus values prior to downstream analysis (64). PCA was performed with command prcomp (CLR-Euclidean ordination). PERMANOVA was performed using vegan commands vegdist (CLR-Euclidean ordination) and adonis2 (66), with patient ID as a strata. Differential abundance was calculated with mixed effects model abundance ~ day + 1 | patient using the nlme command lme, followed by FDR correction, with FDR < 0.2 called as significant. Gene set enrichment analysis was performed on significant genes using clusterProfiler (v4.6.2) command enrichKEGG with a q-value cutoff of 0.2 (68). Line plots were plotted using ggplot2 command geom_smooth with LOESS regression (70).

Generation of ex vivo communities

Three patients from subcohort A with variable *preTA* abundance and Baseline vs C1D7 diversity were selected for ex vivo communities. Brain Heart Infusion supplemented with L-cysteine hydrochloride (0.05% w/v), hemin (5 µg/ml), and vitamin K (1 µg/ml), termed BHI+, was used as media. 100 mg baseline stool from each patient was thawed and added anaerobically to 1 mL BHI+, vortexed for 1 min, and incubated 5 min at RT to allow debris to settle. 500 µL supernatant (“fecal slurry”) was transferred to a new tube. 5-FU was dissolved in dimethylsulfoxide,

supplemented at 1% (v/v) in BHI+ media and assayed at 50 µg/mL. 1% DMSO was added to BHI+ for CAP and vehicle groups; CAP was directly resuspended in this media and assayed at 5 mg/mL. 5 µL fecal slurry was inoculated in sextuplicate into 195 µL of media ± drug in a 96-well plate, with negative control wells to confirm media sterility. Plates were covered with BreathEasy covers and incubated at 37°C for 48 hr in a Gen5 plate reader, with 1 min linear shake prior to OD₆₀₀ readings every 15 min. Plates were removed from plate reader and spun at 3000 rpm for 30 min, followed by supernatant (“spent media”) transfer to a new plate. The plate of cell pellets was frozen at -80°C for future DNA extraction followed by 16S rRNA gene (all samples) and metagenomic sequencing (5-FU-treated communities only).

Extraction of fluoropyrimidine metabolites from ex vivo communities

Spent media was thawed on ice. 50 µL spent media was dissolved in 150 µL water and 800 µL organic phase (50% ACN, 50% MeOH). A standard curve was generated by dissolving serial dilutions of 5-FU in DMSO into BHI+. 10 µL of 50 ng/ml 5-fluorouracil-¹³C,¹⁵N₂ internal standard was spiked into all samples. Samples were vortexed 5 min and incubated on ice for 30 min. Extraction mixture was spun down at 15,000 rcf for 20 min. 250 µL extraction supernatant was dried in speed vac and resuspended in 200 µL of 10% ACN in water for injection.

Extraction of fluoropyrimidine metabolites from stool

Stool was collected from mice and flash-frozen in liquid nitrogen, followed by lyophilization for 27 hours. Dry stool weight was recorded. Dry stool was then homogenized at 4°C with the following settings: 3 x [20 sec 6,400 rpm, 30 sec pause], followed by dissolution in 800 µL of 2:2:1 ACN:MeOH:water. A standard curve was generated by spiking in serial dilutions of CAP and 5-FU in MeOH into stool from untreated mice. 10 µL of 500 ng/ml capecitabine-²H₁₁ and 50 ng/mL 5-fluorouracil-¹³C,¹⁵N₂ in MeOH was spiked into all samples. Samples were vortexed 5 min and incubated on ice for 30 min. Extraction mixture was spun down at 15,000 rcf for 10 min. 250 µL extraction supernatant was dried in the speed vac overnight and resuspended in 1,000 µL of 10% ACN in water. This mixture was centrifuged at 15,000 rcf for 10 minutes, with 100 µL supernatant taken for injection.

LC-MS/MS quantification of CAP and 5-FU

Quantification was performed using a validated fluoropyrimidine quantification protocol (15). Samples were loaded into a Synergi column on a SCIEX Triple Quad 7500 instrument with a linear ion QTRAP. Chromatographic separation was achieved using a Phenomenex Synergi column 4 µM Fusion RP-80 (50 × 2 mm) at 35 °C. The mobile phase was methanol + 0.1% formic acid (A) and HPLC-grade water + 0.1% formic acid (B). A flow rate of 0.4 ml/min was used for the following gradient elution profile: 0% B at 0-2 min, gradient to 100% B from 2-5.9 min, gradient to 0% B at 5.9-6 min. The autosampler was maintained at 4 °C. Eluate from the column was ionized in the LC-MS/MS using an electrospray ionization source in positive polarity. Peak areas were calculated using built-in SCIEX OS software. For quantification from ex vivo communities, 5-FU peak area was normalized to the internal standard, with concentration calculated based on the 5-FU standard curve (Pearson R² = 1.00). For quantification from stool, 5-FU and CAP peak areas

were normalized to the internal standard, with concentration calculated based on the stool spike-in 5-FU and CAP standard curves (Pearson R² = 1.00 and 0.97, respectively).

Reverse-transcription quantitative polymerase chain reaction (RT-qPCR) quantification of *preTA* from culture and mouse stool

E. coli MG1655 strains (*E. coli* Δ*preTA*, wt, *preTA*⁺⁺) used were generated previously (15). For RNA extraction from culture, strains were cultured in quintuplicate in BHI+ overnight, and pelleted at 15,000g. For mouse colonization and RNA extraction from mouse stool, streptomycin water was prepared from autoclaved tap water and supplemented with 5 g/L streptomycin, followed by 0.2 μm filter sterilization. 12 mice were treated *ad libitum* with streptomycin water for the duration of the experiment. Overnight cultures of engineered *E. coli* strains (*E. coli* Δ*preTA*, wt, *preTA*⁺⁺) were pelleted by centrifugation, washed with an equal volume of sterile 0.85% saline, pelleted by centrifugation, and resuspended in 1:10 sterile saline. Mice were gavaged with 200 μL bacterial suspension (4 Δ*preTA*, 4 *preTA*-wt, 4 *preTA*⁺⁺) by gavage following 1 day on strep water. One day post-colonization, stool was collected. Pellets and stool were (re)suspended in 500 μL TRI reagent in Lysing Matrix E tubes, subjected to two rounds of 5 min bead beating, and stored at -80°C. RNA was purified with the Direct-Zol RNA miniprep kit according to the manufacturer protocol and quality was assessed by NanoDrop (A260/A280 = 1.87-2.09, A260/A230=1.92-2.57). cDNA was transcribed using the QuantiTect Reverse Transcription kit per manufacturer protocol. Primers for *preTA* and housekeeping gene *rrsA* were validated and optimized with gradient PCR (table S3). cDNA was serially diluted (1-1,000x) in RNase-free water to remove PCR inhibitors. Each well contained 2 μL cDNA template and 8 μL SYBR master mix with primers (ratio of 1 μL 10 μM forward and reverse primers, 5 μL 2x SYBR Green Master Mix, 2 μL RNase-free water) per well of the 384-well plate. The following qPCR reaction was run: 2 min 50°C, 2 min 95°C, 40 x (15 sec 95°C, 1 min 60°C), melt curve from 65 to 95°C. Relative expression was calculated using the delta-delta Ct method (75).

Mouse studies

All animal experiments were conducted under protocol AN200526 approved by the UCSF Institutional Animal Care and Use Committee. GF C57BL/6J mice were born at UCSF; specific pathogen-free (SPF) C57BL/6J mice were purchased from Jackson Laboratory. Diets were provided *ad libitum*, with standard chow diet (LabDiet 5058) in the SPF facility and standard autoclaved chow diet (LabDiet 5021) in the gnotobiotic facility. Mouse age, sex, and caging is reported in table S2. Mice were housed at temperatures ranging from 67 to 74°F and humidity ranging from 30 to 70% in light/dark cycle 12h/12h with 1-4 mice/cage (exact number of mice per cage for each experiment reported in table S2). GF mice were maintained within the UCSF Gnotobiotic Core Facility. Stool pellets from the Gnotobiotic Core Facility were screened every 2 weeks by culture and qPCR, whenever mice were transferred between isolators, and at the beginning and end of each experiment using V4_515F_Gnoto/V4_806R_Gnoto universal primers (table S3). In CONV-R mice, cage swaps were performed 1 week before experiments to minimize confounding cage-dependent microbiota effects (equal numbers of mice from each original cage were separated into experimental cages split across experimental groups). To enable these cage swaps, we used predominantly female mice (table S2), which are less likely to fight following

changes in their cage mate (76). In the gnotobiotic facility, we used predominantly male mice based on germ-free (GF) mouse availability (table S2).

CAP dose selection

We performed a human-to-mouse dose conversion to account for metabolic differences (from (21)): $2,500 \text{ mg/m}^2 \text{ human dose} \times 1/37 \text{ m}^2/\text{kg} \times 12.3 \text{ human/mouse factor} = 831 \text{ mg/kg mouse dose}$. We titrated up this dose to achieve a reproducible toxicity phenotype, ultimately landing on 1,500 mg/kg. This dose is in line with prior mouse studies of capecitabine pharmacodynamics using 1,000-2,000 mg/kg (22, 77–79). Consistent with our observations, the capecitabine product insert notes that doses of 1,000 mg/kg in mice did not cause significant GI toxicity in pharmaceutical trials, while equivalent doses in humans result in significant GI side effects (80). Lower CAP toxicity in mice relative to humans may be due to metabolic differences (21), microbiome differences, or increased dihydropyrimidine dehydrogenase activity in intestinal tissue (55).

CAP delivery in murine models

Buffer was prepared by dissolving 964 mg sodium citrate dihydrate and 139 mg of citric acid into 90 mL deionized water (DI), adjusting pH to 6.0 with HCl or NaOH, adding 5 g gum arabic, bringing final volume to 100 mL, and autoclaving for 20 min. CAP solution was prepared fresh daily (SPF experiments) or weekly (gnotobiotic experiments) by dissolving CAP into the buffer with continuous agitation and heating. Mice were given a single CAP bolus daily by oral gavage for all experiments except the CAP regional profiling experiment, where mice were gavaged twice daily. CAP was dosed by body weight, with CAP quantity determined such that 200 μL solution contained the CAP gavage dose (500, 1,100 or 1,500 mg/kg) for the largest mouse. Gavage needles were rinsed with DI in between each mouse, with different needles for each experimental group.

CAP regional profiling experiment

11 mixed-sex mice were singly housed for one week, then gavaged with 500 mg/kg CAP ($n = 6$ total, 3 per sex) or 200 μL vehicle buffer ($n = 5$ total, 3 female, 2 male) twice daily at 7AM and 7PM (total CAP dosage of 1,000 mg/kg/day) for two weeks. Mice were weighed daily, with no changes noted in vehicle vs CAP or over time (two-way ANOVA $p>0.05$). Baseline stool and endpoint stool, jejunum, ileum, cecum, proximal colon, and distal colon contents were collected, followed by DNA extraction and 16S rRNA gene sequencing.

Establishment of CAP toxicity experiment

20 mice were gavaged with 1,500 mg/kg CAP ($n = 12$) or 200 μL buffer ($n = 8$) once daily. Half the mice were sacrificed at Day 4, with remaining mice sacrificed at Day 12. Endpoint small intestine, cecum, and colon contents were collected. 5 metrics were used to assess toxicity. (i) *Weight loss and survival time*. Mice were weighed daily and sacrificed at 15% weight loss (“survival time”) or at experimental endpoint, whichever came first. (ii) *Anatomic measurements*. Mouse colon length, small intestine length, spleen weight, and gonadal fat pad weight were

measured. (iii) *Body composition*. Mouse body composition was measured at Days 0, 4, and 12 by EchoMRI with primary accumulation time of 1 minute. (iv) *Lipocalin-2 ELISA*. Enzyme-linked immunosorbent assay was performed with Mouse Lipocalin-2/NGAL DuoSet ELISA kit using the manufacturer's protocol with the following modifications. Preweighed colon contents (50-100 mg) were combined with 1 mL PBS + 0.1% Tween 20 and vortexed for 20 min, then centrifuged for 10 min at 4°C and 12,000 rcf. For sample wells, 20 µL of extracted sample was added to 100 µL of reagent diluent and 6-fold serially diluted. For standard wells, 125 pg/mL mouse lipocalin-2 standard with 2-fold serial dilutions was used, with two blank wells. Absolute concentrations were calculated with linear fit to a log-log plot of mouse Lcn-2 concentration versus OD. (v) *Hand-foot syndrome*. Thermal hind paw hyperalgesia was measured as described (22). Briefly, mice were placed on a 52°C hotplate and latency to rear paw lick, rear paw flick, or jump was recorded. *Sequencing*. We performed metagenomic sequencing of stool samples collected on Day 0 and Day 4. We focused on these samples to determine whether CAP-induced microbiota changes manifest by Day 4 and to maximize our statistical power to detect differences (20 stool samples were available at Day 4, whereas only 10 were available at Day 12 by design.)

Broad-spectrum antibiotic CAP toxicity experiment

Antibiotic (AVNM) or Vehicle (Veh) water was prepared fresh weekly from autoclaved tap water supplemented with sucrose (0.5 g/L sucrose) ± antibiotics (1 g/L ampicillin, 0.5 g/L vancomycin, 1 g/L neomycin, 0.5 g/L metronidazole), followed by 0.2 µm filter sterilization. 24 mice were treated *ad libitum* with AVNM ($n = 12$) or Veh ($n = 12$) water for the duration of the experiment. After 1 week of antibiotics, mice were treated with 1,500 mg/kg CAP daily for 2 weeks. Weight was measured daily, and stool was taken at Days -7, 0, 3, and 5 (relative to CAP start). Endpoint small intestine, cecum, and colon contents were collected. Endpoint cecal contents weight and gonadal fat pad weight were measured. To assess bacterial load, fecal slurries were generated by adding 100 mg Day 0 stool into 1 mL BHI+, vortexing for 1 min, and allowing fecal debris to settle for 5 min. 10 µL of supernatant was 10x serially diluted in BHI+, with 2.5 µL of each dilution spotted on BHI+ agar plates and incubated at 37°C for 5 days to quantify colony forming units (CFUs). All stool work was performed anaerobically.

Germ-free vs conventional microbiota CAP toxicity experiment

To generate CONV-D mice, cecal contents from a single SPF donor was resuspended in 10% BHI+ aerobically and passed through a 100 µm filter, with 200 µL administered to GF mice followed by a 1-week engraftment period. CONV-R ($n = 8$), CONV-D ($n = 8$), and GF ($n = 8$) mice were treated with 1,100 mg/kg CAP daily for 2 weeks. Weight was measured daily. Endpoint small intestine contents, cecal contents, colon contents, and large intestine length were collected for all mice, with endpoint small intestine length, spleen weight, cecal contents weight, and gonadal fat pad weight collected for CONV-D and GF mice.

preTA CAP rescue experiments

Two independent experiments were conducted. In each, streptomycin water was prepared fresh weekly from autoclaved tap water supplemented with 5 g/L streptomycin, followed by 0.2 µm filter sterilization. 32 mice (Experiment 1, fig. S13) or 36 mice (Experiment 2, **Fig. 5**) were treated

ad libitum with streptomycin water for the duration of the experiment. Overnight cultures of engineered *E. coli* strains (*E. coli* Δ *preTA*, wt, *preTA*⁺⁺) were pelleted by centrifugation, washed with an equal volume of sterile 0.85% saline, pelleted by centrifugation, and resuspended in 1:10 sterile saline. Mice were gavaged with 200 μ L bacterial suspension (Experiment 1: 16 Δ *preTA*, 16 *preTA*⁺⁺; Experiment 2: 12 Δ *preTA*, 12 wt, 12 *preTA*⁺⁺) by gavage following 1 day on strep water. One day post-colonization (“Day 0”), mice began 2 weeks of treatment with 1,500 mg/kg CAP daily. Weight was measured daily and stool was taken at Days -1, 0, and at sacrifice. Endpoint small intestine, cecum, and colon contents were collected, along with colon length. Fecal slurries were generated by anaerobically adding 100 mg Day 0 stool into 1 mL LB + strep, vortexing 1 min, and allowing fecal debris to settle for 5 min. 10 μ L of supernatant was 10-fold serially diluted in LB + strep, with 2.5 μ L of each dilution spotted on Eosin Methylene Blue (EMB) agar plates and incubated anaerobically at 37°C for 1 day to quantify *E. coli* CFUs.

Gnotobiotic *preTA* CAP rescue experiment

Overnight cultures of engineered *E. coli* strains (*E. coli* Δ *preTA* and *E. coli* *preTA*⁺⁺) were pelleted by centrifugation, washed with an equal volume of sterile 0.85% saline, pelleted by centrifugation again and resuspended in 1:10 sterile saline. Mice were gavaged with 200 μ L bacterial suspension or saline only ($n = 6$ *E. coli* Δ *preTA*, $n = 6$ *E. coli* *preTA*⁺⁺, $n = 6$ “mock”). One-week post-colonization, stool was collected, and mice began 2 weeks of treatment with 1,500 mg/kg CAP daily, with weight measured daily. Endpoint small intestine length and colon length were measured. Endpoint *E. coli* CFUs from Day 0 stool were quantified by culturing on MacConkey Agar as described previously (15). For group comparisons, Δ *preTA* and mock colonized mice were binned together into “mock/ Δ *preTA*” (both contain no *preTA*).

Capecitabine stool pharmacokinetics experiment

Streptomycin water was prepared from autoclaved tap water and supplemented with 5 g/L streptomycin, followed by 0.2 μ m filter sterilization. 12 mice were treated *ad libitum* with streptomycin water for the duration of the experiment. Overnight cultures of engineered *E. coli* strains (*E. coli* Δ *preTA*, wt, *preTA*⁺⁺) were pelleted by centrifugation, washed with an equal volume of sterile 0.85% saline, pelleted by centrifugation, and resuspended in 1:10 sterile saline. Mice were gavaged with 200 μ L bacterial suspension (6 Δ *preTA*, 6 *preTA*⁺⁺) by gavage following 1 day on strep water. One day post-colonization, baseline stool was collected, and mice were gavaged with 1,500 mg/kg CAP at 9AM. Stool was collected at 3-, 5-, and 7-hours post-gavage for CAP and 5-FU quantification.

Gnotobiotic humanization CAP toxicity experiments

Two independent experiments were conducted. For each experiment, two donors with variable baseline *preTA* were selected to humanize 16 gnotobiotic mice ($n = 8$ per donor; 1 isolator per donor). Fecal slurries were generated anaerobically by adding 100 mg stool to 2 mL PBS, vortexing, and letting the mixture settle for 5 min. 1.5 mL of supernatant (“fecal slurry”) was transferred to a new tube on ice. 100 μ L fecal slurry was orally gavaged into each mouse, with the researcher blinded to colonization group. One week post-colonization, baseline stool was collected and mice began 2 weeks of treatment with 1,500 mg/kg CAP daily. Weight was measured daily.

Endpoint stool, small intestine contents, cecal contents, colon contents, colon length, spleen weight, and gonadal fat pad weights were collected. Baseline stool was subjected to metagenomic sequencing to assess *preTA* status. For group comparisons, mice with no detected K17722/K17723 were called “*preTA* low”, with others called “*preTA* high.” Where stool was not evaluable (1/32 mice), mice were called as the *preTA* abundance of their cagemates.

SUPPLEMENTAL FIGURES AND LEGENDS

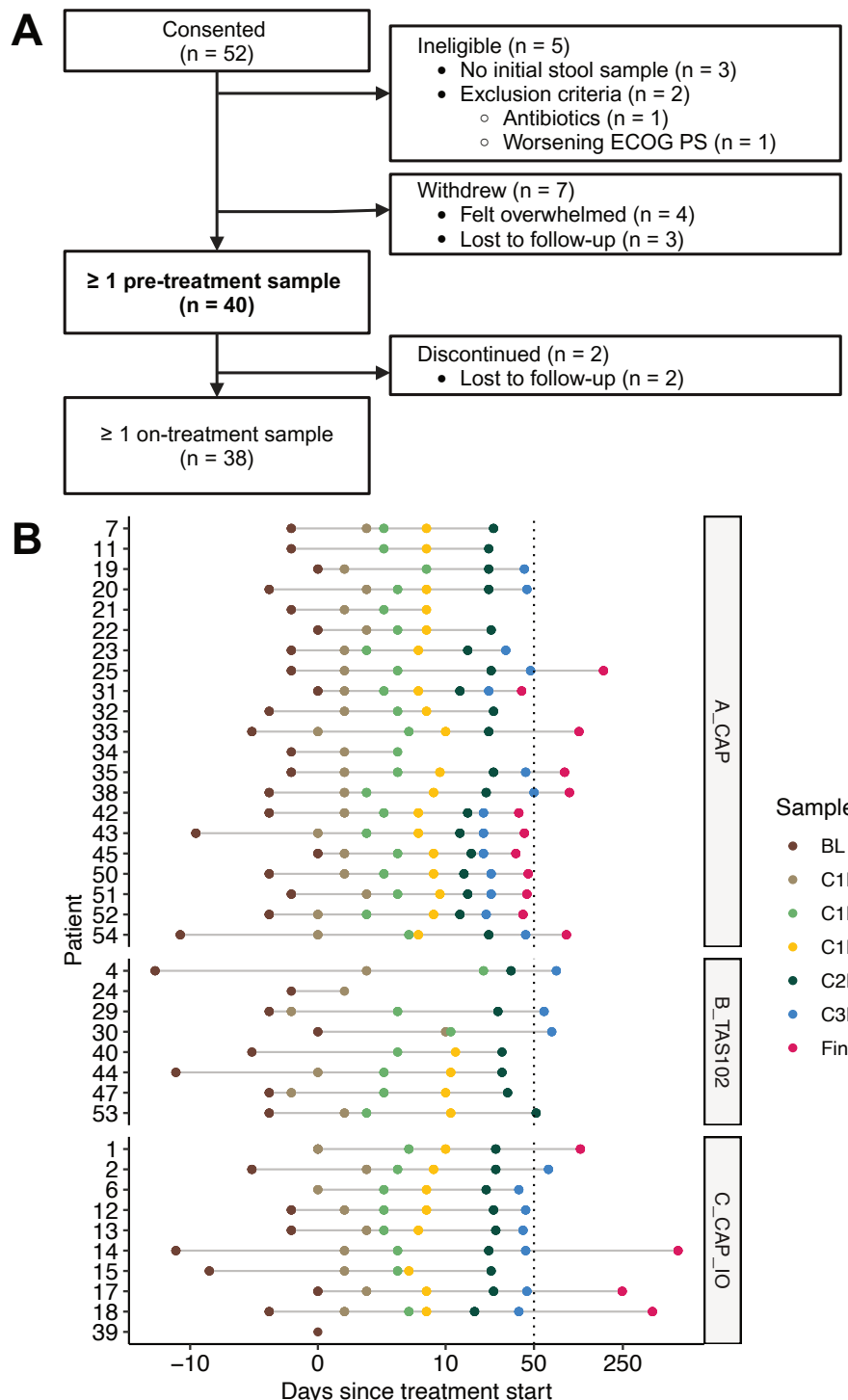


Figure S1: GO study design. (A) Flow diagram of patients consented to GO study. **(B)** Day of evaluable stool samples from each patient relative to day 0, the first day of cycle 1 of chemotherapy. Each dot represents a single stool sample, and each color represents a study-defined timepoint. Samples to the right of the vertical dotted line at day 50 were excluded from mixed-effects modeling. The x-axis is pseudo-log transformed.

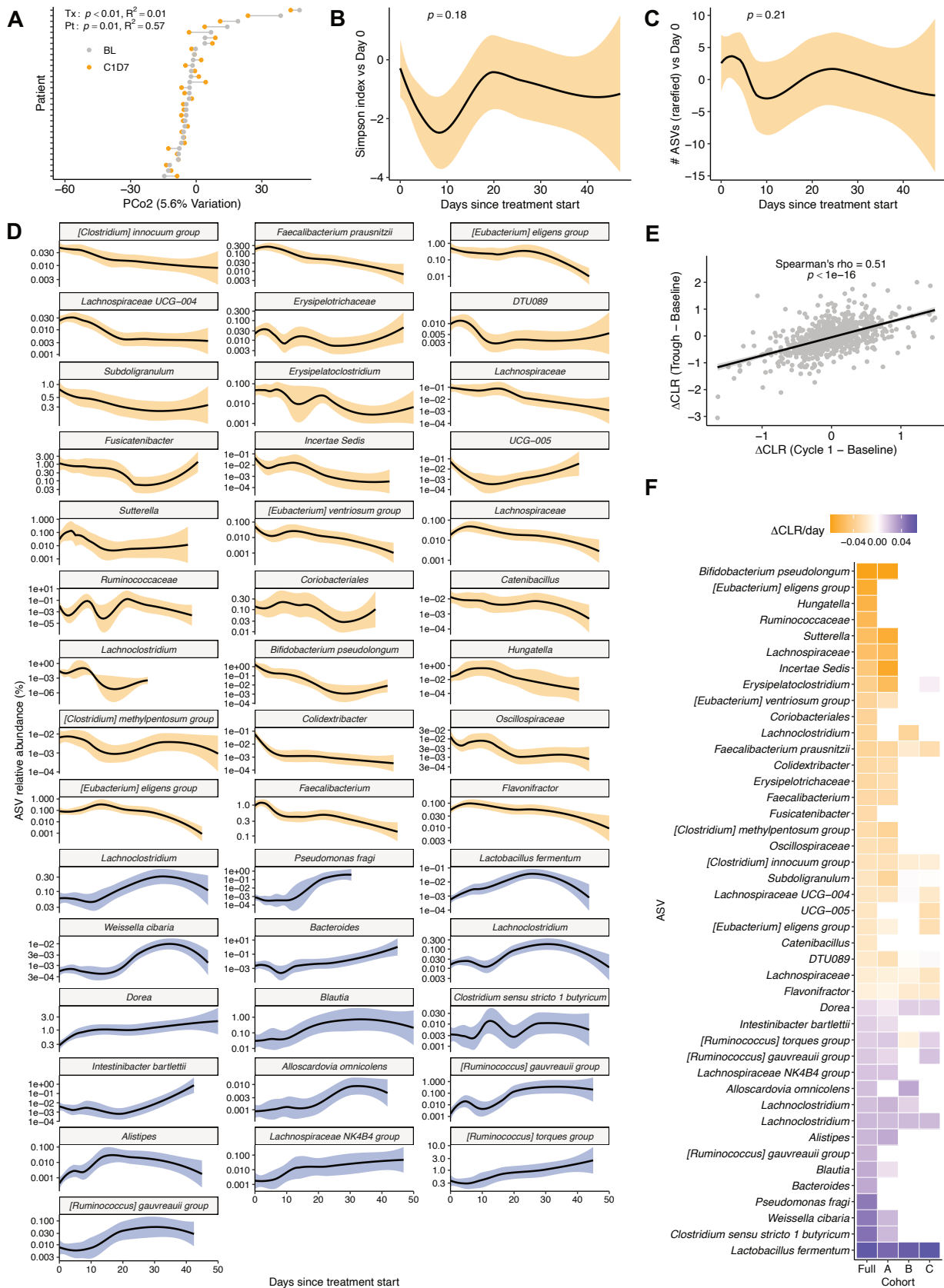


Figure S2: Oral fluoropyrimidine treatment impacts gut microbiome composition in GO study patients. **(A)** Reproducible shifts in gut bacterial amplicon sequence variants (ASV) are observed across study participants between BL and C1D7 samples on the second principal coordinate (PCo2) of central log ratio (CLR)-transformed Euclidean distances. *P* value: PERMANOVA with patient ID as stratum, all samples. **(B,C)** Alpha diversity metrics inverse Simpson index **(B)** and number of ASVs **(C)** during the study, normalized to baseline. *P* values: mixed-effects model, diversity \sim day + 1 | patient. **(D)** Time course of all significantly altered ASVs from **Fig. 1C**, with ASVs that increased/decreased during treatment in blue/orange, respectively. Solid lines with shading represent LOESS interpolation means \pm SEM. **(E)** Correlation between taxa changes observed in Cycle 1 and Trough relative to Baseline. *P* value: Spearman's rank correlation. **(F)** Heatmap of differential ASV abundance in the full cohort and each subcohort. Displayed ASVs are those that are significantly altered in the full cohort (**Fig. 1C**). Shading color indicates treatment effect (orange, depleted with treatment; blue, enriched), with white indicating the ASV was detected in fewer than 3 patients in the subcohort.

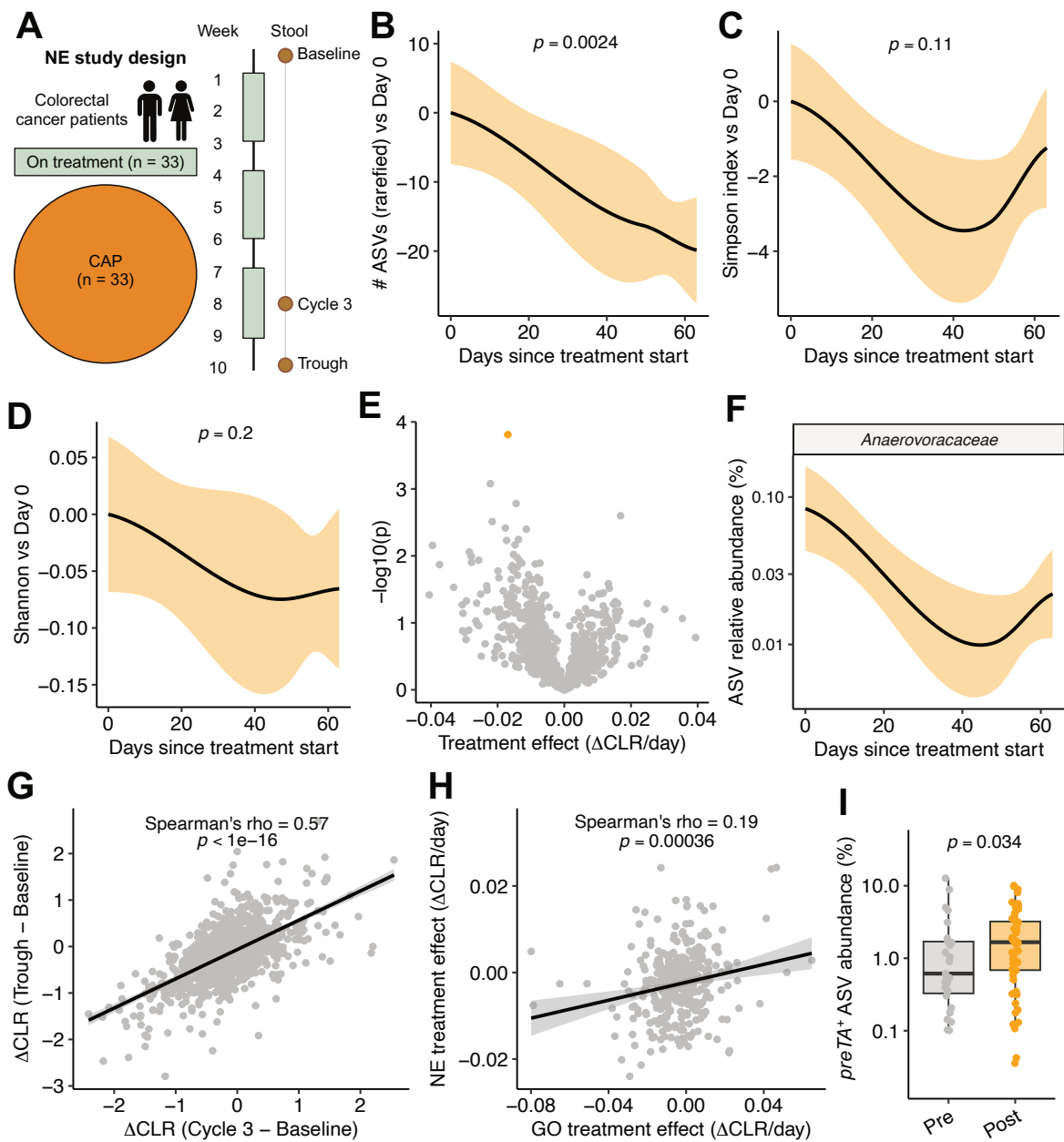


Figure S3: Oral fluoropyrimidine treatment impacts gut microbiome composition in a European cohort of patients with colorectal cancer. (A) Netherlands (NE) study design depicting patients treated with capecitabine (CAP). (B-D) Change in alpha diversity metrics number of rarefied ASVs (B), inverse Simpson index (C), Shannon index (D) during the study, normalized to baseline. P values: mixed-effects model, diversity ~ day + 1 | patient. (E) Volcano plot of bacterial amplicon sequence variants (ASVs) with respect to treatment time (mixed-effects model, central log ratio (CLR)-transformed abundance ~ day + 1 | patient). Orange represents the only significantly depleted ASV after treatment [false discovery rate (FDR) < 0.2]. (F) Time course of significantly altered *Anaerovoracaceae* ASV. (G) Correlation between taxa changes observed in Cycle 3 and Trough relative to Baseline. (H) Correlation between taxa changes observed in GO and NE studies. (I) Sum of *preTA⁺* *Escherichia*, *Anaerostipes*, *Eubacterium*, *Citrobacter* ASV relative abundances. P value: one-sided Mann-Whitney U test. (B-D,F): Solid lines with shading represent LOESS interpolation mean ± SEM. (G,H): Solid lines with shading represent a linear regression best fit with 95% confidence interval, with Spearman correlation P values.

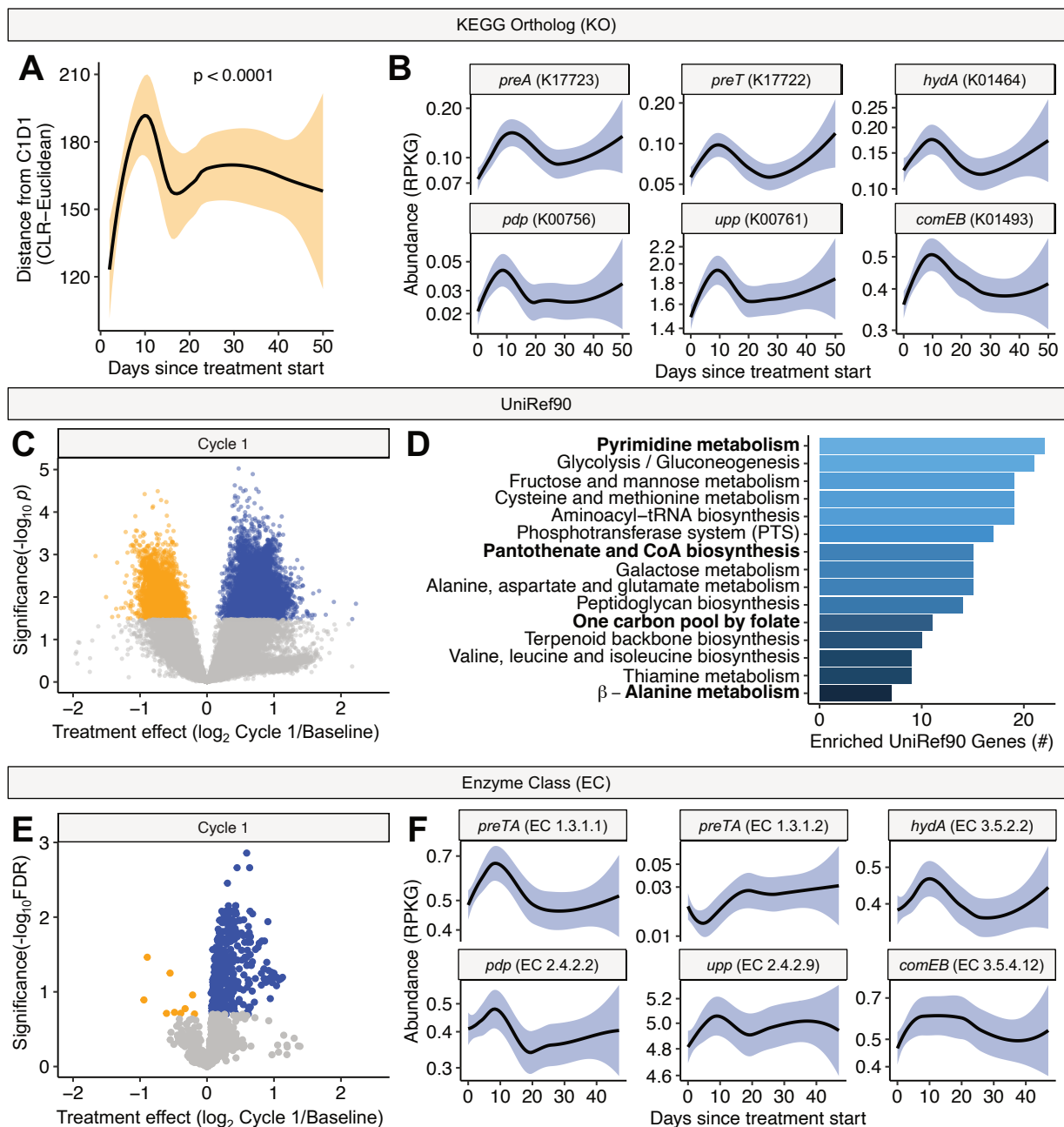


Figure S4: Oral fluoropyrimidine treatment selects for pyrimidine metabolism genes. (A) Microbial community distance to cycle 1 day 1 location calculated per-patient (central log ratio-Euclidean ordination). P value: mixed-effects model, distance \sim day + 1 | patient. (B) Time course of significantly altered KO gene families from pyrimidine metabolism, pantothenate and CoA biosynthesis, and β -alanine metabolism pathways. (C) Volcano plot of UniRef90 gene families detected in at least 50% of samples with respect to treatment time. Points represent significantly enriched (blue) and depleted (orange) gene families ($FDR < 0.2$). (D) Gene set enrichment analysis of significantly enriched UniRef90 gene families from (C). UniRef90 gene sets with $p < 0.1$ are displayed. Fluoropyrimidine metabolism-related pathways are bolded. (E) Volcano plot of Enzyme Classes (EC) detected in at least 50% of samples with respect to treatment time. Points represent significantly enriched (blue) and depleted (orange) ECs ($FDR < 0.2$). (F) Time course of ECs corresponding to genes from (B). (A,B,F) Solid line with shading represents LOESS interpolation mean \pm SEM.

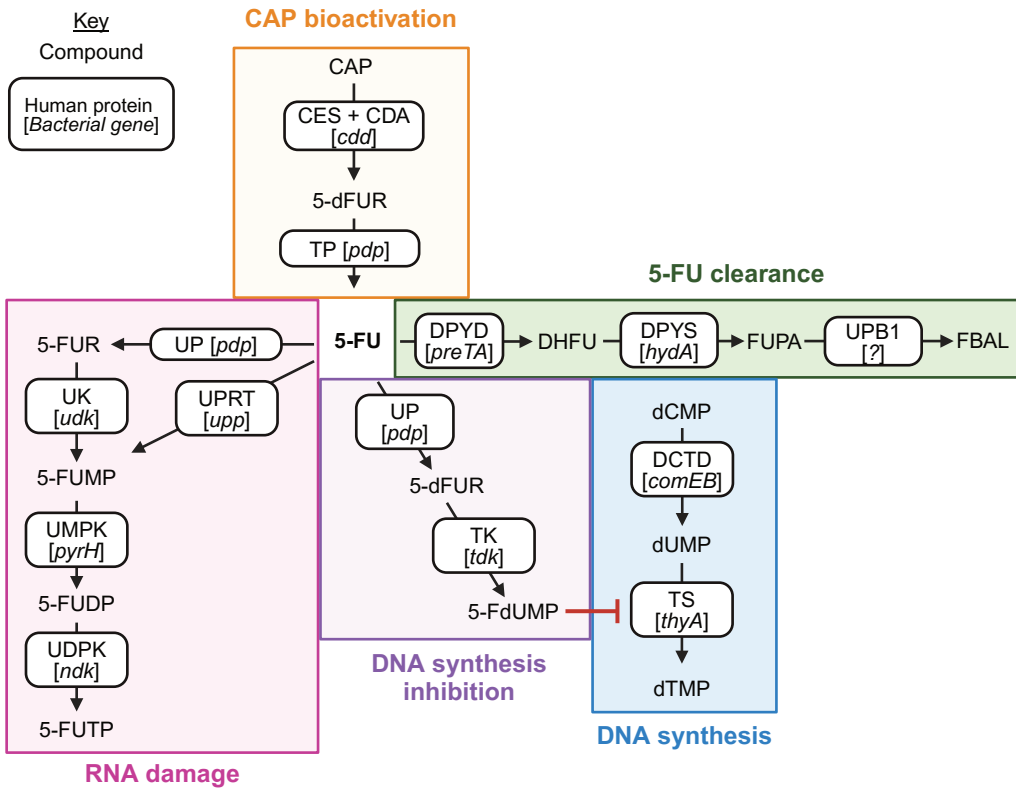


Figure S5: Fluoropyrimidine bioactivation and metabolism. Created with BioRender.com. Text in boxes represents enzymes responsible for a transformation, formatted as human protein [*bacterial gene*]. Text outside boxes represents fluoropyrimidine metabolites. Arrows indicate directionality to produce terminal metabolites responsible for cytotoxicity or clearance, but do not indicate that a reaction is irreversible.

CAP bioactivation. In humans, capecitabine (CAP) is de-esterified into 5-DFCR by liver carboxyesterase (CES), followed by deamination into 5-dFUR by liver and tumor cytidine deaminase (CDA) (81). In bacteria, *Bacillus subtilis* *cdd* encodes a tetrameric cytidine deaminase that directly converts CAP to 5-dFUR, a capacity also shared by other enzymes cloned from gut metagenomic sequences (82). In humans, thymidine phosphorylase (TP) converts 5-dFUR to 5-FU (81); in bacteria, pyrimidine nucleoside phosphorylase genes (*pdp*, including *upp* in *E. coli*) encode the responsible enzymes (5, 83).

5-FU clearance. In humans and bacteria, 5-FU is cleared to DHFU by homologous dihydropyrimidine dehydrogenases (DPYD, encoded by *preTA* in bacteria including *E. coli* and *Anaerostipes hadrus*) (15). DHFU is further converted to FUPA by homologous dihydropyrimidases (DPYS, encoded by *A. hadrus* *hydA*) (10). In humans, FUPA is then converted to fluoro-beta-alanine (FBAL) by beta-ureidopropionase (UPB1) prior to renal clearance (84).

DNA synthesis. *De novo* DNA synthesis requires conversion of dUMP to dTMP by thymidylate synthase (TS, encoded by *E. coli* *thyA*) (85). Upstream, dCMP stores can be converted to dUMP by dCMP deaminase (DCTD, encoded by *B. subtilis* *comEB*) (86).

DNA synthesis inhibition. DNA synthesis inhibition is a primary mechanism-of-action of 5-FU (87). In humans and bacteria, 5-FU is converted to 5-dFUR by uridine phosphorylase (UP, encoded by bacterial *pdp* including *E. coli* *udp*), which is then converted to 5-FdUMP by thymidine kinase (TK, encoded by *E. coli* *tdk*) (88). 5-FdUMP then forms an inhibitory ternary complex with thymidylate synthase (TS, encoded by *E. coli* *thyA*), blocking DNA synthesis (85).

RNA damage. In humans and bacteria, 5-FU is converted directly to 5-FUMP by UPRT (UPRT, encoded by *E. coli* and *Mycobacterium spp.* *upp*) (15, 89). Alternatively, 5-FU can be converted to 5-FUR by uridine phosphorylase (UP, encoded by bacterial *pdp* including *E. coli* *udp*), which is then converted to 5-FUMP by uridine kinase (UK, encoded by *E. coli* *udk*) (88). 5-FUMP is sequentially phosphorylated to 5-FUDP and 5-FUTP by uridine monophosphate kinase (UMPK, encoded by *E. coli* *pyrH*) and uridine diphosphate kinase (UDPK, encoded by *E. coli* *ndk*) (88). 5-FUTP disrupts RNA processing, resulting in cytotoxicity (90).

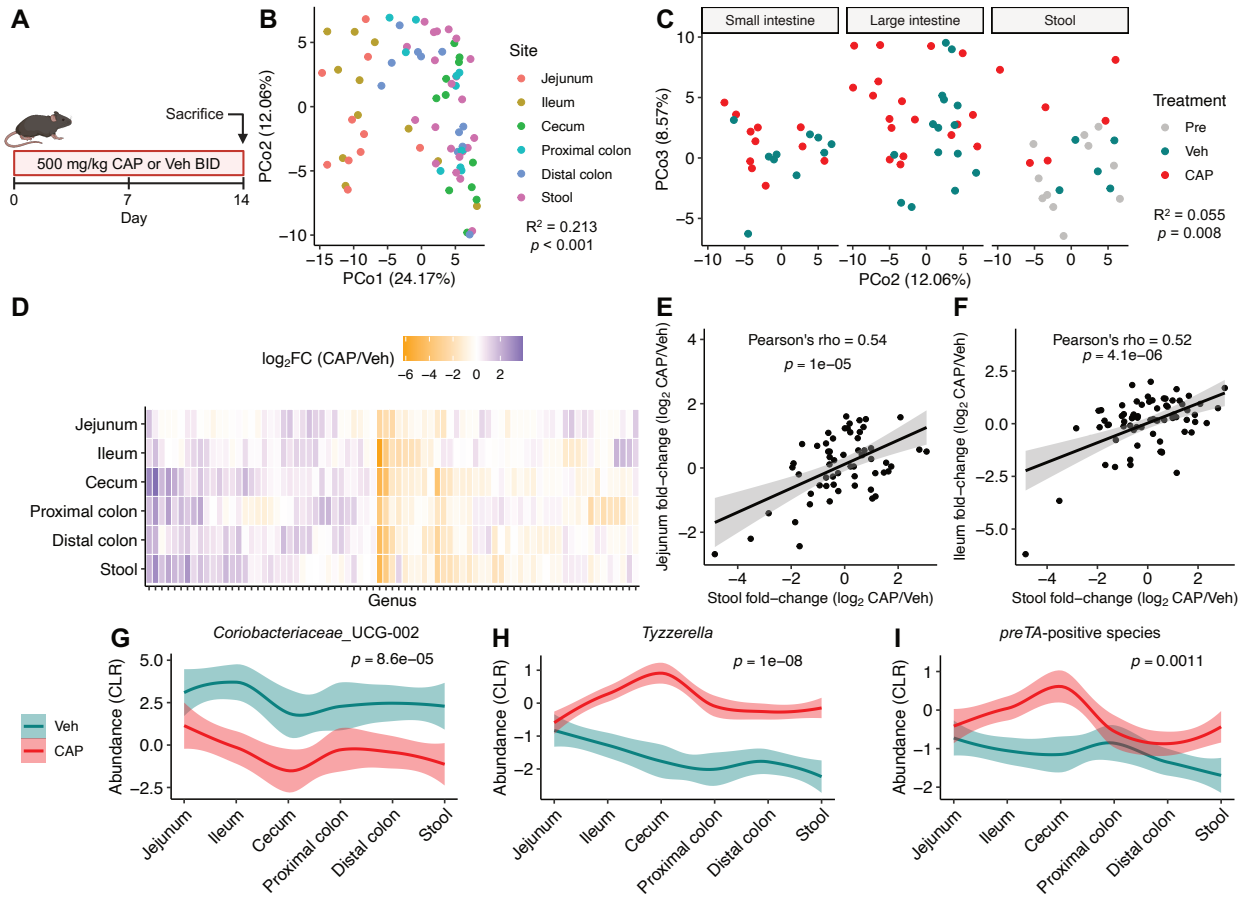


Figure S6: CAP alters murine gut microbiota composition along the gastrointestinal (GI) tract. (A) CAP GI mouse model. Mixed-sex mice were gavaged daily with 500 mg/kg CAP ($n = 6$) or Vehicle (Veh, $n = 5$) twice daily (BID), for a total of 1,000 mg/kg CAP/day. Stool was collected at Day 0, and all gastrointestinal contents (jejunum, ileum, cecum, proximal colon, distal colon, stool) were collected at Day 14. (B) Bacterial genera compositions separate by body site using principal coordinate analysis (PCoA) with central log ratio (CLR)-transformed Euclidean distances. P value: PERMANOVA with mouse ID as stratum. (C) Bacterial genera compositions separate by treatment per body site (Small intestine: Jejunum, Ileum; Large intestine: Cecum, Proximal colon, Distal colon; Stool) using PCoA with CLR-Euclidean distances. P value: PERMANOVA of all data combined with mouse ID as stratum. (D) Heatmap of endpoint differential genera abundance for each body site, with genera ordered by hierarchical clustering (Ward D2). (E-F) Correlation between taxa changes observed in jejunum (E) or ileum (F) vs stool. P value: Pearson's correlation. (G-I) Abundance of most depleted genus in stool (G), most enriched genus in stool (H), and *preTA*-positive species across body sites (I). P values: mixed-effects model, abundance ~ treatment + 1 | tissue. Solid line with shading represents LOESS interpolation mean \pm SEM.

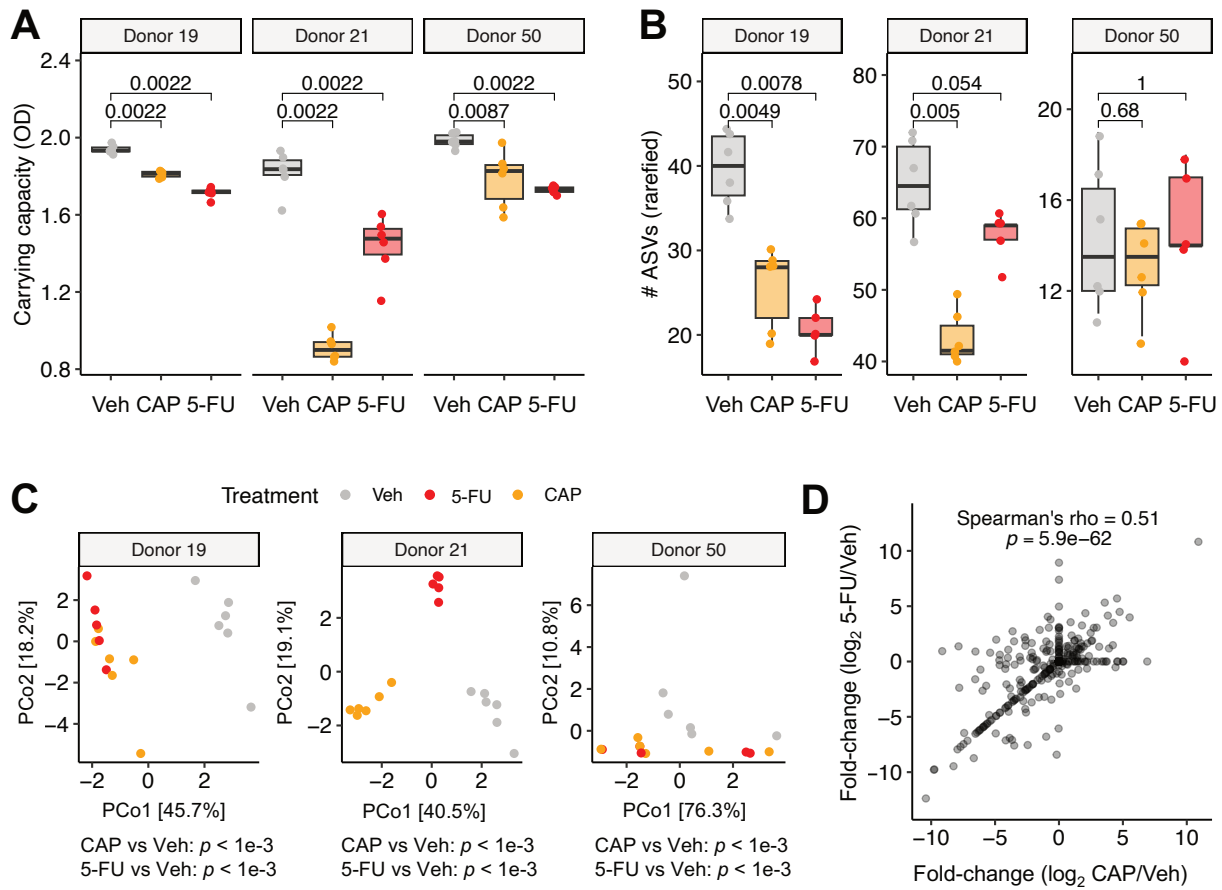


Figure S7: Fluoropyrimidines alter human gut microbiota composition ex vivo. **(A)** Carrying capacity (optical density at 600 nm, OD₆₀₀) and **(B)** alpha diversity (number of amplicon sequence variants, ASVs) of stool-derived ex vivo communities incubated with Vehicle (Veh), CAP, or 5-FU. *P* value: Mann-Whitney *U* test. **(C)** Principal coordinate plots of ASV abundances for ex vivo communities incubated with Veh, 5-FU, or CAP [central log ratio (CLR)-Euclidean ordination]. *P* value: Treatment PERMANOVA relative to Vehicle. **(D)** CAP- and 5-FU-induced changes in amplicon sequence variant abundance are highly correlated. *P* value: Spearman correlation. Each point represents a single ex vivo community **(A-C)** or a single amplicon sequence variant across communities from a given donor **(D)**. To calculate log₂ fold change, a pseudocount of 0.00001 abundance was added to the numerator and denominator. For all, $n = 5$ biological replicate communities were generated from each of $n = 3$ donors.

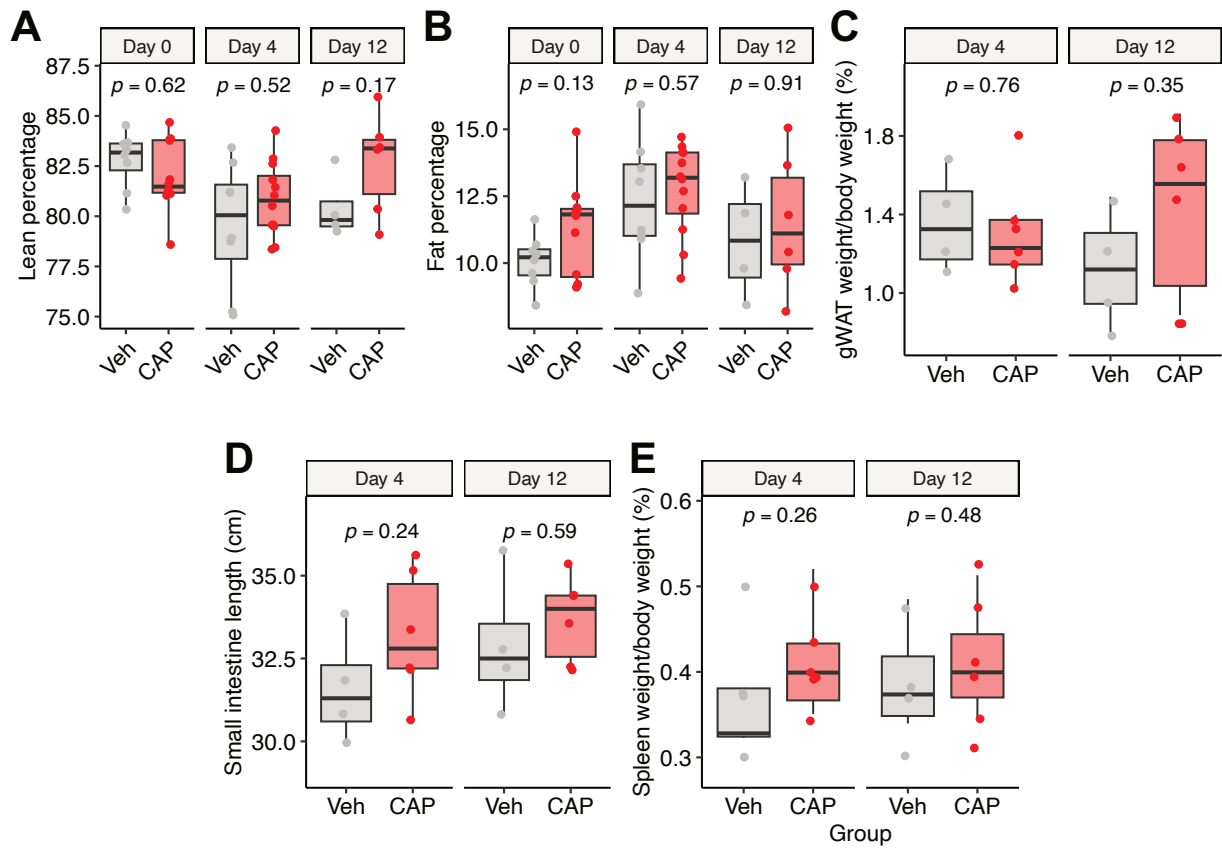


Figure S8: A mouse model of capecitabine (CAP) toxicity. (A-B) Body composition by EchoMRI at Day 0, Day 4 and Day 12 of CAP treatment for $n = 8$ Vehicle (Veh) and $n = 12$ CAP-treated mice: lean percentage (A) and fat percentage (B). Toxicity endpoints at Day 4 and Day 12 of CAP treatment ($n = 4$ Veh and $n = 6$ CAP mice sacrificed at each day): gonadal white adipose tissue (gWAT) weight/body weight (C), small intestine length (D), and spleen weight/body weight (E). P values: Mann-Whitney U test, CAP vs Veh.

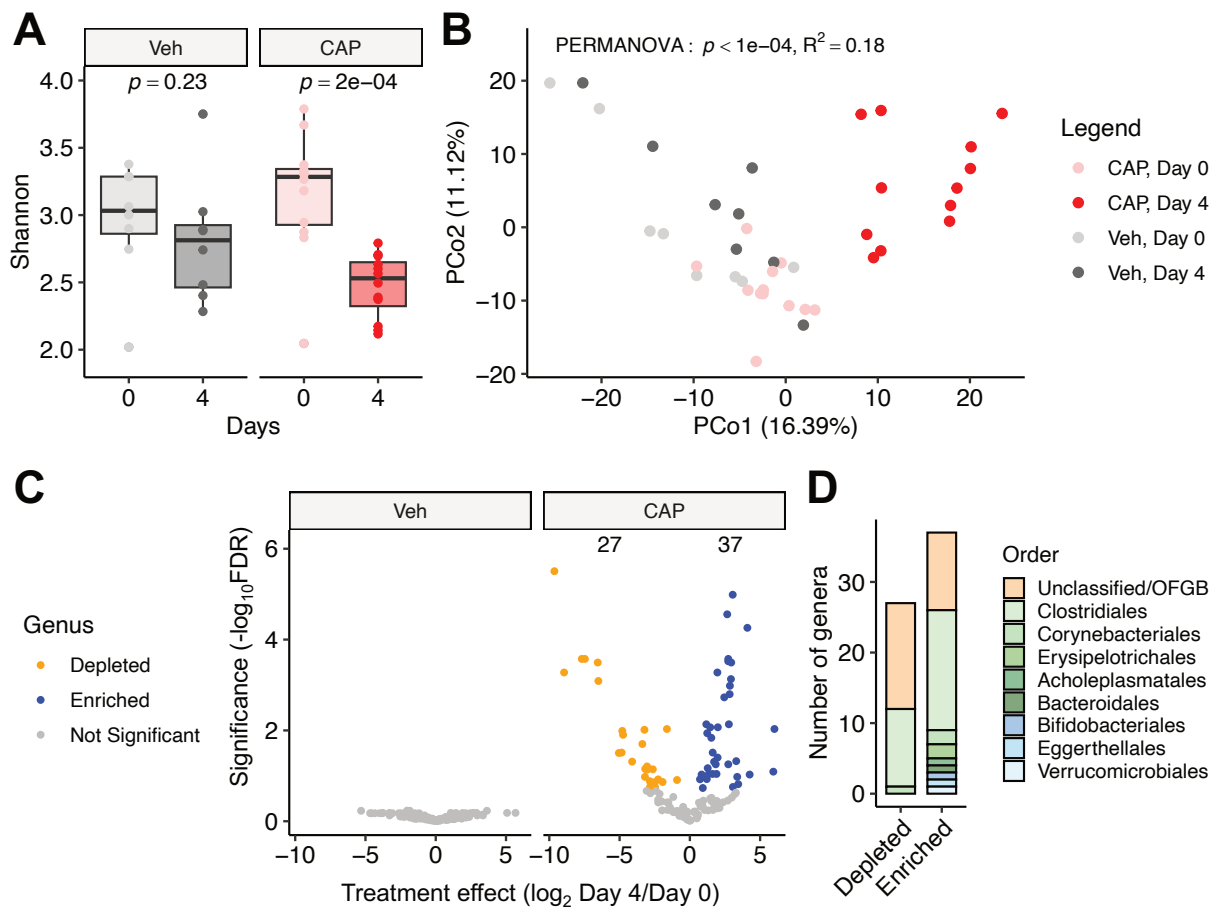


Figure S9: Capecitabine (CAP) alters murine gut microbiota composition in a toxicity model. (A) Shannon index during the experiment. P value: Mann-Whitney U test. (B) Shifts in gut bacterial genera are observed between Day 0 and 4 in CAP-treated mice using principal coordinate analysis (PCoA) of central log ratio (CLR)-transformed Euclidean distances. P value: PERMANOVA with Mouse ID as stratum. (C) Volcano plot of bacterial genera with respect to treatment time, comparing Day 0 and 4. P value: mixed-effects model, CLR-transformed abundance \sim day + 1 | mouse. Points represent enriched (blue) and depleted (orange) genera after treatment [false discovery rate (FDR) < 0.2]. (D) Order membership of enriched and depleted genera from (C). All panels incorporate data from $n = 8$ Vehicle (Veh)- and $n = 12$ CAP-treated mice.

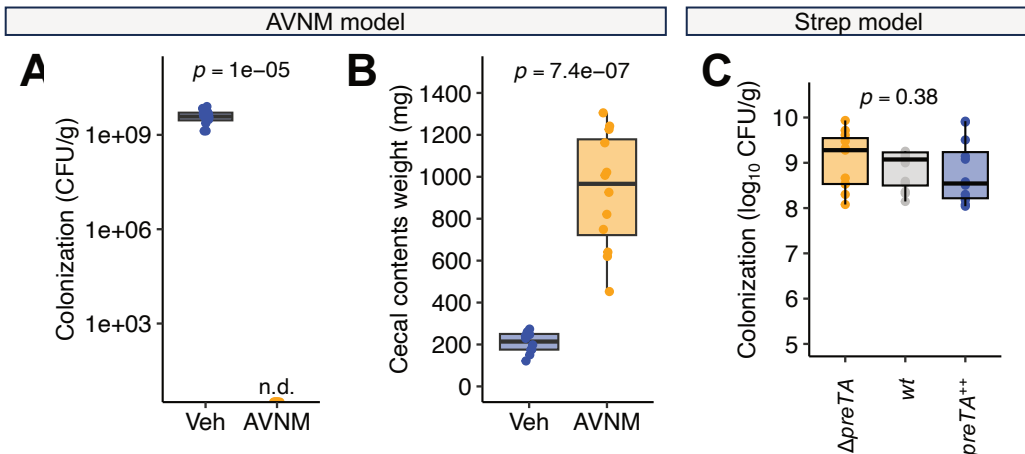


Figure S10: Microbial load in antibiotic depletion models. (A-B) An ampicillin, vancomycin, neomycin, and metronidazole (AVNM) cocktail depletes the gut microbiota of $n = 12$ Vehicle (Veh)-treated mice relative to $n = 12$ AVNM-treated mice, measured using stool colonization at Day 0 (1 week post-AVNM) (A) and cecal contents weight at sacrifice (B). (C) *E. coli* $\Delta preTA$, wt, and $preTA^{++}$ similarly colonize mice treated with 5 g/L streptomycin ($n = 12$ mice/colonization group). P values: Mann-Whitney U test (A,B), Kruskal-Wallis test (C).

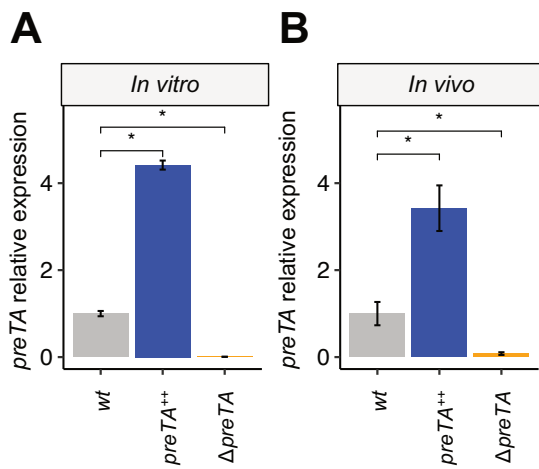


Figure S11: *preTA*⁺⁺ *E. coli* transcript levels are significantly higher than *wt* *E. coli*. *preTA* expression levels in pure culture ($n = 3$ cultures/strain) **(A)** and mice treated with 5 g/L streptomycin followed by colonization ($n = 4$ mice/colonization group) **(B)**. All expression values were normalized to housekeeping gene *rrsA*, then divided by mean *wt* *preTA* expression. Values are mean \pm SEM, * $P < 0.05$, Mann-Whitney *U* test.

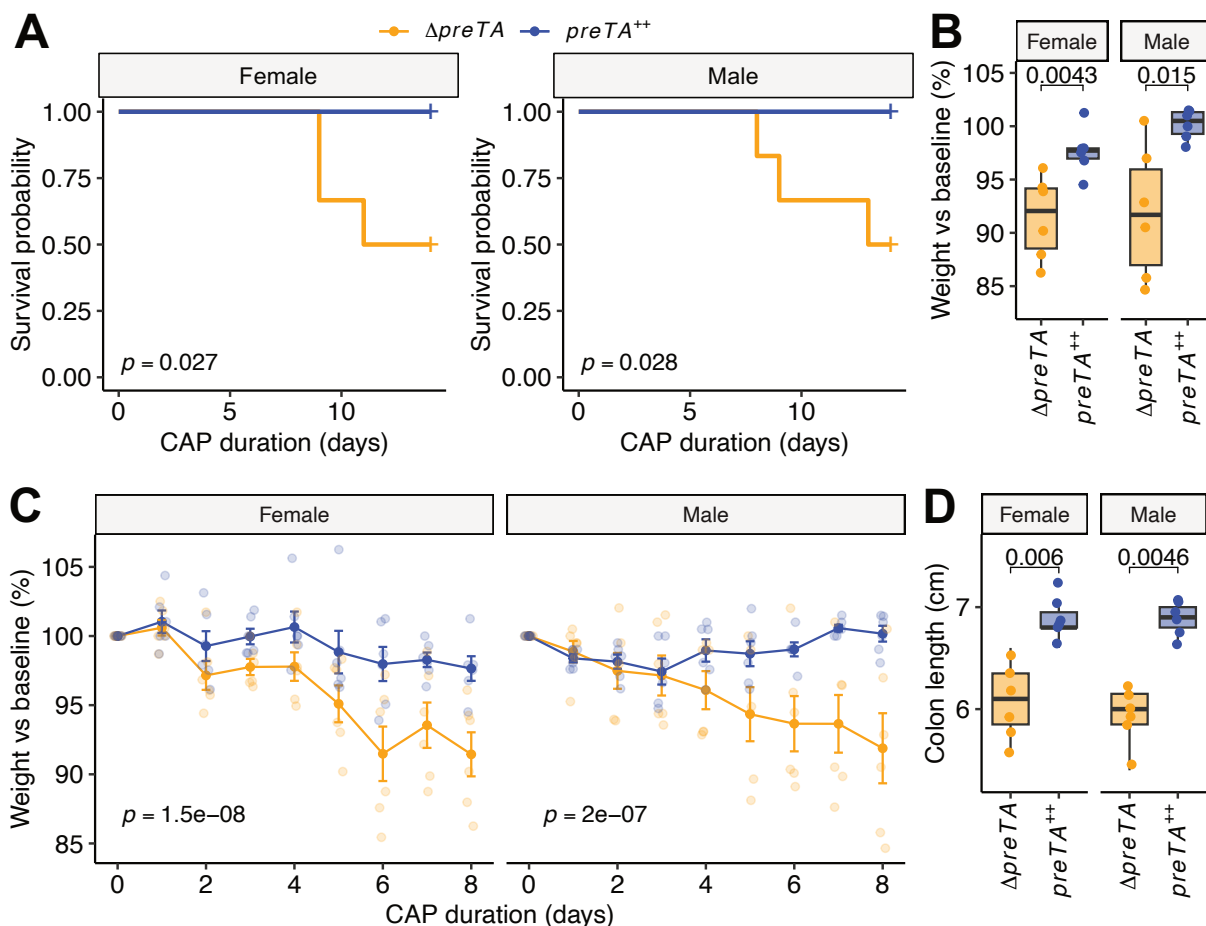


Figure S12: Bacterial *preTA* rescues capecitabine (CAP) toxicity in both male and female mice. Mixed-sex mice were treated with streptomycin for 1 day, gavaged with *E. coli* ΔpreTA ($n = 12$) or preTA^{++} ($n = 12$), then gavaged daily with 1,500 mg/kg CAP (same data as Figs. 5A-D). (A) CAP survival curves. (B) Mouse weight on Day 8 relative to baseline. (C) CAP-induced weight loss over time. (D) Endpoint colon lengths. P values: one-sided Mantel-Cox test (A), Mann-Whitney U test (B,D), group term from two-way ANOVA (C).

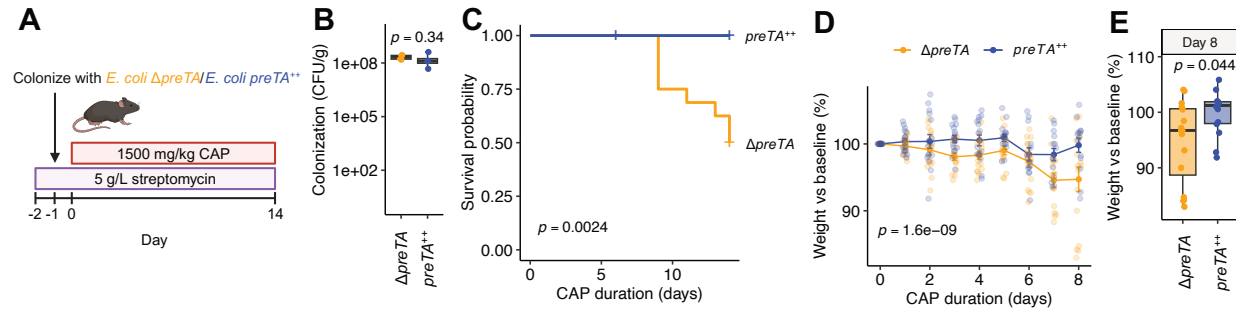


Figure S13: Bacterial *preTA* rescues capecitabine (CAP) toxicity in a streptomycin-treated mouse model. (A) *preTA* streptomycin (strep) colonization CAP toxicity model in female-only C57BL/6J mice (separate experiment from Fig. 5). Female mice were treated with streptomycin for 1 day, gavaged with *E. coli* Δ preTA ($n = 16$) or preTA⁺⁺ ($n = 16$), then gavaged daily with 1,500 mg/kg CAP. **(B)** *E. coli* colonization level by cage. **(C)** Survival curve. **(D-E)** CAP-induced weight loss **(D)** and weight on Day 8 **(E)**. *P* values: Mann-Whitney *U* test **(B,E)**, Mantel-Cox test **(C)**, group term from two-way ANOVA **(D)**.

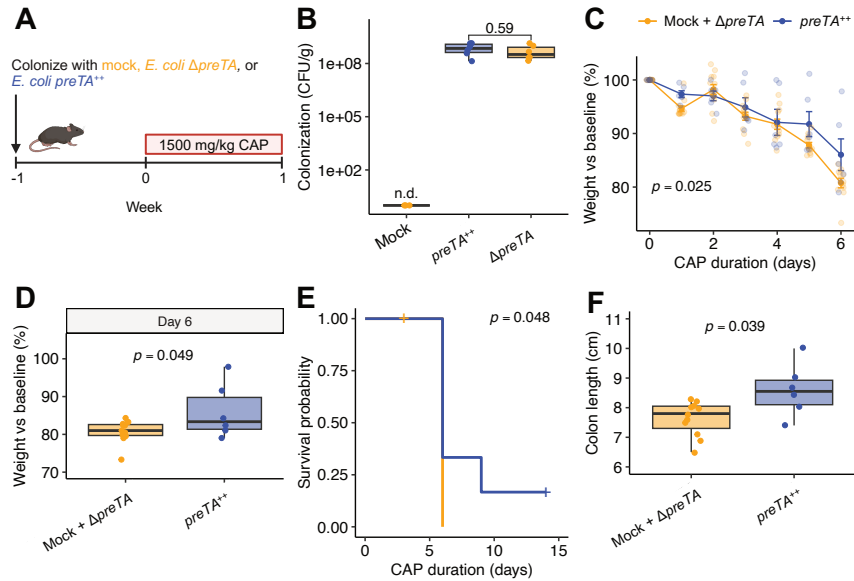


Figure S14: Bacterial preTA rescues capecitabine (CAP) toxicity in a gnotobiotic mouse model. (A) Experimental design of gnotobiotic mice colonized with mock ($n = 6$), Δ preTA *E. coli* ($n = 6$), or preTA⁺⁺ *E. coli* ($n = 6$) for 1 week prior to treatment with 1,500 mg/kg CAP daily by oral gavage. (B) *E. coli* stool colonization level at baseline. n.d. = not detected. (C) CAP-induced weight loss. P value: two-way ANOVA. (D) Mouse weight on Day 6. P value: one-way ANOVA. (E) Survival curve. P value: Mantel-Cox test. (F) Colon length at sacrifice. (B,F): P value: Mann-Whitney U Test.

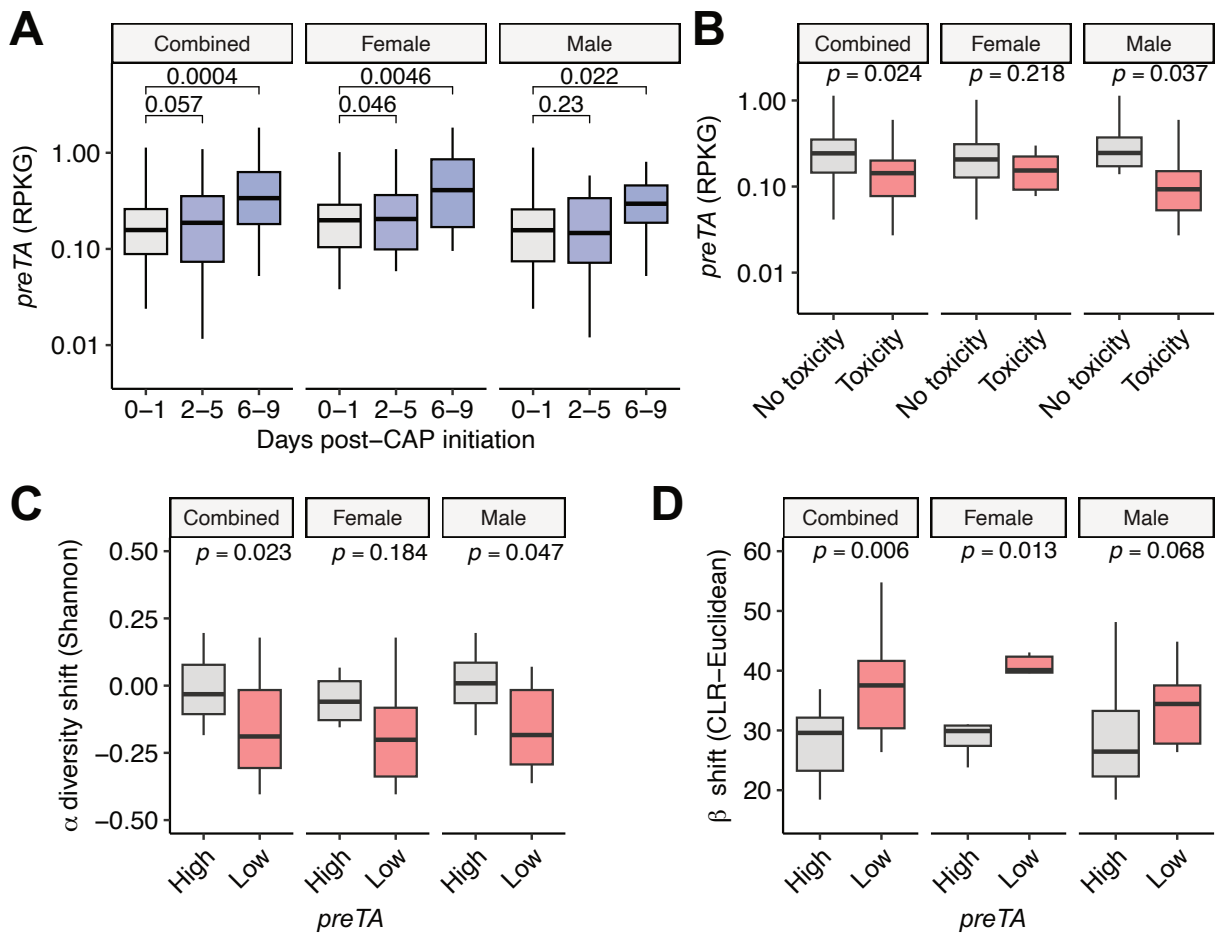


Figure S15: Capecitabine-*preTA* interactions are detectable for each sex. (A) *preTA* levels during Cycle 1 of CAP treatment. *P* value: one-sided paired Student's *t* test. **(B)** Patients experiencing toxicity have lower baseline stool bacterial *preTA* levels ($n = 40$ combined, 20 male, 20 female). *P* value: one-sided Mann-Whitney *U* test. **(C)** *preTA* level (above/below mean) vs change in alpha diversity during Cycle 1 (C7D1-C1D1 Shannon index, $n = 30$ combined, 18 male, 12 female). **(D)** *preTA* level (above/below mean) vs change in beta diversity during Cycle 1 (C7D1-C1D1 CLR-Euclidean distance, $n = 30$ combined, 18 male, 12 female). **(C,D)** *P* value: one-sided Wilcoxon signed-rank test.

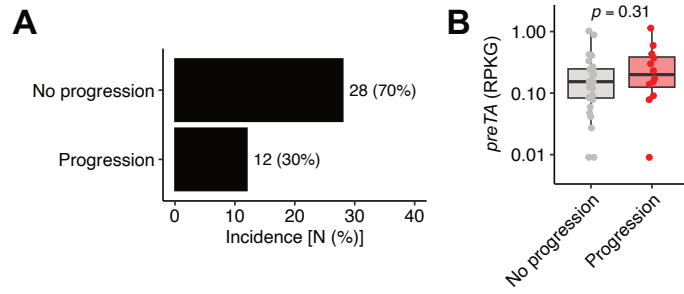


Figure S16: Bacterial *preTA* is not associated with tumor progression. (A) Documented tumor progression during Cycles 1-3 in GO patients ($n = 40$). (B) Patients experiencing tumor progression have similar baseline stool bacterial *preTA* levels ($n = 40$). P value: Mann-Whitney U test.

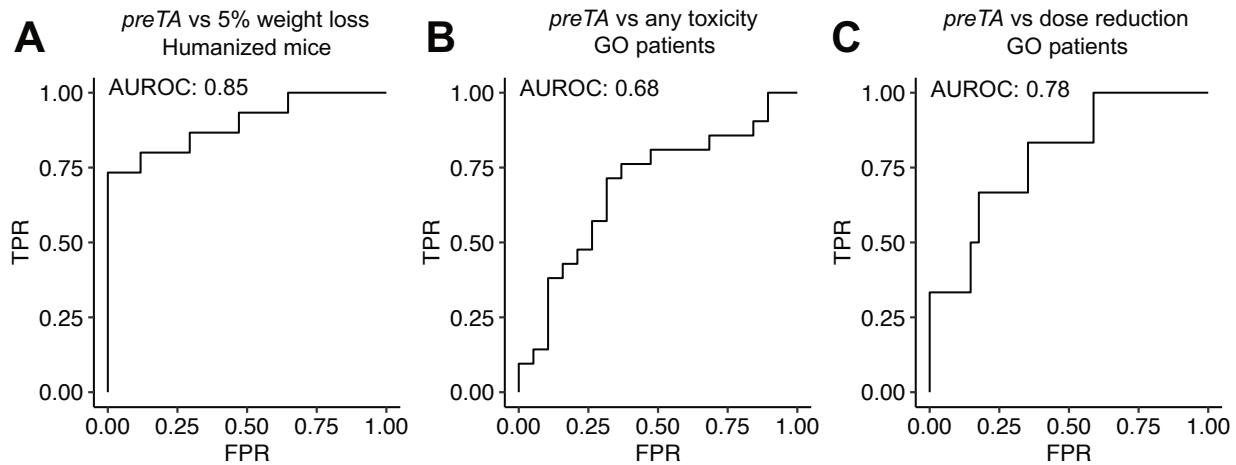


Figure S17: Bacterial *preTA* predicts CAP toxicity. Univariate receiver operating characteristic (ROC) curves for classification of $\geq 5\%$ weight loss in humanized mice ($n = 32$ mice from 4 colonization groups across 2 independent experiments) (A), any documented toxicity in GO patients ($n = 40$) (B), and dose reductions in GO patients ($n = 40$) (C), all using *preTA* abundance. True positive rate (TPR), false positive rate (FPR), and area under the receiver operating characteristic curve (AUROC) are reported.

SUPPLEMENTAL TABLES

Table S1: Baseline clinical characteristics of GO study patients. Values are displayed as median (interquartile range) for continuous variables and *n* for categorical variables. Data is for the 40 patients who submitted at least 1 stool sample.

Age (years)	52.5 (10.5)
BMI (kg/m²)	24.8 (4.8)
Sex	
Female	20
Male	20
Race (self-reported)*	
Asian	4
Black/African American	2
Unknown	3
White	32
Ethnicity (self-reported)	
Hispanic or Latino	3
Not Hispanic or Latino	34
Unknown	3
Subcohort and concurrent pharmacologic treatment	
A: CAP as SOC	21
<i>CAP + oxaliplatin</i>	9
<i>CAP + radiation</i>	9
<i>CAP + bevacizumab</i>	2
<i>CAP + non-specified concurrent therapy</i>	1
B: TAS102	9
<i>TAS102 monotherapy</i>	5
<i>TAS102 + bevacizumab</i>	2
<i>TAS102 + Y-90 radioembolization</i>	2
C: CAP + bevacizumab + pembrolizumab	10
<i>CAP + bevacizumab + pembrolizumab</i>	10

Location of primary tumor	
Cecum/ascending	7
Transverse	6
Descending/Sigmoid	11
Rectosigmoid	3
Rectum	13
TNM Stage at diagnosis	
I	2
II	4
III	22
IV	11
Unknown	1
Prior surgical resection of primary	
Yes	27
No	13
Ostomy	
Colostomy (present)	2
Colostomy (reversed)	2
Ileostomy (present)	1
None	35
Metastases present	
Yes	21
No	19

*Total = 41 since 1 patient self-identified as multiple races.

Table S2: Mouse experiment metadata. Age is mean \pm SEM at Day 0. CAP dose is daily total.

Experiment	Group	n	Sex	Strain	Age (weeks)	Housing (n/cage)	LabDiet	CAP dose (mg/kg)
Mechanisms of Toxicity	Vehicle	8	F	C57BL/6J	9	4	5058	1500
Mechanisms of Toxicity	CAP	12	F	C57BL/6J	9	4	5058	0
Antibiotic Depletion	Vehicle	12	F	C57BL/6J	11.3	4	5058	1500
Antibiotic Depletion	AVNM	12	F	C57BL/6J	11.3	4	5058	1500
Conventionalization	CONV-R	8	F	C57BL/6J	8.1	4	5058	1100
Conventionalization	GF	8	F	C57BL/6J	13.6 \pm 0.3	4	5021	1100
Conventionalization	CONV-D	8	F	C57BL/6J	13.3 \pm 0.3	4	5021	1100
CAP Regional Profiling Exp	Vehicle	3	F	C57BL/6J	7	1	5058	0
CAP Regional Profiling Exp	CAP	3	F	C57BL/6J	7	1	5058	1000
CAP Regional Profiling Exp	Vehicle	2	M	C57BL/6J	7	1	5058	0
CAP Regional Profiling Exp	CAP	3	M	C57BL/6J	7	1	5058	1000
SPF <i>preTA</i> Rescue Exp 2	Δ <i>preTA</i>	6	F	C57BL/6J	6.3	3	5058	1500
SPF <i>preTA</i> Rescue Exp 2	<i>preTA</i> wt	6	F	C57BL/6J	6.3	3	5058	1500
SPF <i>preTA</i> Rescue Exp 2	<i>preTA</i> ⁺⁺	6	F	C57BL/6J	6.3	3	5058	1500
SPF <i>preTA</i> Rescue Exp 2	Δ <i>preTA</i>	6	M	C57BL/6J	6.3	3	5058	1500
SPF <i>preTA</i> Rescue Exp 2	<i>preTA</i> wt	6	M	C57BL/6J	6.3	3	5058	1500
SPF <i>preTA</i> Rescue Exp 2	<i>preTA</i> ⁺⁺	6	M	C57BL/6J	6.3	3	5058	1500
SPF <i>preTA</i> Rescue Exp 1	Δ <i>preTA</i>	16	F	C57BL/6J	7.3	4	5058	1500
SPF <i>preTA</i> Rescue Exp 1	<i>preTA</i> ⁺⁺	16	F	C57BL/6J	7.3	4	5058	1500
SPF Stool PK	Δ <i>preTA</i>	6	F	C57BL/6J	9.3	4	5058	1500
SPF Stool PK	<i>preTA</i> ⁺⁺	6	F	C57BL/6J	9.3	4	5058	1500
SPF <i>preTA</i> qRT-PCR	Δ <i>preTA</i>	4	F	C57BL/6J	9.3	4	5058	0
SPF <i>preTA</i> qRT-PCR	<i>preTA</i> wt	4	F	C57BL/6J	9.3	4	5058	0
SPF <i>preTA</i> qRT-PCR	<i>preTA</i> ⁺⁺	4	F	C57BL/6J	9.3	4	5058	0
Gnoto <i>preTA</i> Rescue	GF	6	M	C57BL/6J	7.5 \pm 0.4	1-3	5021	1500
Gnoto <i>preTA</i> Rescue	Δ <i>preTA</i>	6	M	C57BL/6J	8.1 \pm 0.4	1-3	5021	1500
Gnoto <i>preTA</i> Rescue	<i>preTA</i> ⁺⁺	6	M	C57BL/6J	8.1	1-3	5021	1500
GO Humanization Exp 1	Donor 35	8	M	C57BL/6J	9.8 \pm 0.5	1-3	5021	1500
GO Humanization Exp 1	Donor 32	8	M	C57BL/6J	9.7 \pm 0.5	1-3	5021	1500
GO Humanization Exp 2	Donor 7	8	M	C57BL/6J	11.5 \pm 0.1	1-3	5021	1500
GO Humanization Exp 2	Donor 39	8	M	C57BL/6J	11.4 \pm 0.1	1-3	5021	1500

Table S3: Primer sequences.

Primer name	Supplier	Sequence (5' to 3')
16S V4_515Fmod_Nextera	Azenta	TCGTCGGCAGCGTCAGATGTGTATAAGAGACAGGTGYCAG CMGCCGCGTAA
16S V4_806Rmod_Nextera	Azenta	GTCTCGTGGGCTCGGAGATGTGTATAAGAGACAGGGACTA CNVGGGTWTCTAAT
16S V4_515F_Gnoto	Azenta	GTGCCAGCMGCCGCGTAA
16S V4_806R_Gnoto	Azenta	GGACTACHVGGGTWTCTAAT
preTA_F	Azenta	CGAGGCGATTCACTCACTATTT
preTA_R	Azenta	AACCTGTGTCGTAGGCTTT
rrsA_F	Azenta	GCGCGTCTGAAAGAAAGGTT
rrsA_R	Azenta	CTGCCATCGGTTCCCTTTA

References (including main text)

1. P. Y. Muller, M. N. Milton, The determination and interpretation of the therapeutic index in drug development. *Nat. Rev. Drug Discov.* **11**, 751–761 (2012).
2. Q. Ma, A. Y. H. Lu, Pharmacogenetics, pharmacogenomics, and individualized medicine. *Pharmacol. Rev.* **63**, 437–459 (2011).
3. B. Tamraz, A. P. Venook, DPYD Pharmacogenetics: To Opt-in or to Opt-out. *JCO Oncol Pract* **20**, OP2400255 (2024).
4. M. Zimmermann, M. Zimmermann-Kogadeeva, R. Wegmann, A. L. Goodman, Mapping human microbiome drug metabolism by gut bacteria and their genes. *Nature* **570**, 462–467 (2019).
5. B. Javdan, J. G. Lopez, P. Chankhamjon, Y.-C. J. Lee, R. Hull, Q. Wu, X. Wang, S. Chatterjee, M. S. Donia, Personalized Mapping of Drug Metabolism by the Human Gut Microbiome. *Cell* **181**, 1661-1679.e22 (2020).
6. K. R. Trepka, C. A. Olson, V. Upadhyay, C. Zhang, P. J. Turnbaugh, Pharma[e]cology: How the Gut Microbiome Contributes to Variations in Drug Response. *Annu. Rev. Pharmacol. Toxicol.* **65** (2024), doi:10.1146/annurev-pharmtox-022724-100847.
7. K. D. Miller, L. Nogueira, T. Devasia, A. B. Mariotto, K. R. Yabroff, A. Jemal, J. Kramer, R. L. Siegel, Cancer treatment and survivorship statistics, 2022. *CA Cancer J. Clin.* **72**, 409–436 (2022).
8. M. W. Saif, N. A. Katirtzoglou, K. N. Syrigos, Capecitabine: an overview of the side effects and their management. *Anticancer Drugs* **19**, 447–464 (2008).
9. D. R. Budman, Capecitabine. *Invest. New Drugs* **18**, 355–363 (2000).
10. D. Liu, L.-S. Xie, S. Lian, K. Li, Y. Yang, W.-Z. Wang, S. Hu, S.-J. Liu, C. Liu, Z. He, Anaerostipes hadrus, a butyrate-producing bacterium capable of metabolizing 5-fluorouracil. *mSphere* **9**, e00816-23 (2024).
11. C. A. T. C. Lunenburg, L. M. Henricks, H.-J. Guchelaar, J. J. Swen, M. J. Deenen, J. H. M. Schellens, H. Gelderblom, Prospective DPYD genotyping to reduce the risk of fluoropyrimidine-induced severe toxicity: Ready for prime time. *Eur. J. Cancer* **54**, 40–48 (2016).
12. B. A. W. Jacobs, M. J. Deenen, M. Joerger, H. Rosing, N. de Vries, D. Meulendijks, A. Cats, J. H. Beijnen, J. H. M. Schellens, A. D. R. Huitema, Pharmacokinetics of Capecitabine and Four Metabolites in a Heterogeneous Population of Cancer Patients: A Comprehensive Analysis. *CPT Pharmacometrics Syst Pharmacol* **8**, 940–950 (2019).
13. B. A. Jennings, Y. K. Loke, J. Skinner, M. Keane, G. S. Chu, R. Turner, D. Epurescu, A. Barrett, G. Willis, Evaluating predictive pharmacogenetic signatures of adverse events in colorectal cancer patients treated with fluoropyrimidines. *PLoS One* **8**, e78053 (2013).

14. S. Piawah, T. S. Kyaw, K. Trepka, A. L. Stewart, R. V. Mora, D. Stanfield, K. Levine, E. L. Van Blarigan, A. Venook, P. J. Turnbaugh, T. Nguyen, C. E. Atreya, Associations between the Gut Microbiota, Race, and Ethnicity of Patients with Colorectal Cancer: A Pilot and Feasibility Study. *Cancers* **15**, 4546 (2023).
15. P. Spanogiannopoulos, T. S. Kyaw, B. G. H. Guthrie, P. H. Bradley, J. V. Lee, J. Melamed, Y. N. A. Malig, K. N. Lam, D. Gempis, M. Sandy, W. Kidder, E. L. Van Blarigan, C. E. Atreya, A. Venook, R. R. Gerona, A. Goga, K. S. Pollard, P. J. Turnbaugh, Host and gut bacteria share metabolic pathways for anti-cancer drug metabolism. *Nat Microbiol* **7**, 1605–1620 (2022).
16. R. Aarnoutse, J. Ziemons, J. de Vos-Geelen, L. Valkenburg-van Iersel, A. C. L. Wildeboer, A. Vievermans, G.-J. M. Creemers, A. Baars, H. J. H. M. J. Vestjens, G. N. Le, D. J. M. Barnett, S. S. Rensen, J. Penders, M. L. Smidt, The Role of Intestinal Microbiota in Metastatic Colorectal Cancer Patients Treated With Capecitabine. *Clin. Colorectal Cancer* **21**, e87–e97 (2022).
17. G. A. O'Donovan, J. Neuhard, Pyrimidine metabolism in microorganisms. *Bacteriol. Rev.* **34**, 278–343 (1970).
18. B. Rosener, S. Sayin, P. O. Oluoch, A. P. García González, H. Mori, A. J. Walhout, A. Mitchell, Evolved bacterial resistance against fluoropyrimidines can lower chemotherapy impact in the *Caenorhabditis elegans* host. *eLife* **9** (2020), doi:10.7554/eLife.59831.
19. D. Rosmarin, C. Palles, D. Church, E. Domingo, A. Jones, E. Johnstone, H. Wang, S. Love, P. Julier, C. Scudder, G. Nicholson, A. Gonzalez-Neira, M. Martin, D. Sargent, E. Green, H. McLeod, U. M. Zanger, M. Schwab, M. Braun, M. Seymour, L. Thompson, B. Lucas, V. Boige, N. Ribelles, S. Afzal, H. Enghusen, S. A. Jensen, M.-C. Etienne-Grimaldi, G. Milano, M. Wadelius, B. Glimelius, H. Garmo, M. Gusella, T. Lecomte, P. Laurent-Puig, E. Martinez-Balibrea, R. Sharma, J. Garcia-Foncillas, Z. Kleibl, A. Morel, J.-P. Pignon, R. Midgley, D. Kerr, I. Tomlinson, Genetic markers of toxicity from capecitabine and other fluorouracil-based regimens: investigation in the QUASAR2 study, systematic review, and meta-analysis. *J. Clin. Oncol.* **32**, 1031–1039 (2014).
20. E. Lkhagva, H.-J. Chung, J. Hong, W. H. W. Tang, S.-I. Lee, S.-T. Hong, S. Lee, The regional diversity of gut microbiome along the GI tract of male C57BL/6 mice. *BMC Microbiol.* **21**, 44 (2021).
21. A. B. Nair, S. Jacob, A simple practice guide for dose conversion between animals and human. *J. Basic Clin. Physiol. Pharmacol.* **7**, 27–31 (2016).
22. B. Yang, X. Xie, D. Lv, J. Hu, Y. Chen, Z. Wu, S. Luo, S. Zhang, Capecitabine induces hand-foot syndrome through elevated thymidine phosphorylase-mediated locoregional toxicity and GSDME-driven pyroptosis that can be relieved by tipiracil. *Br. J. Cancer* **128**, 219–231 (2023).
23. V. Gopalakrishnan, C. N. Spencer, L. Nezi, A. Reuben, M. C. Andrews, T. V. Karpinets, P. A. Prieto,

- D. Vicente, K. Hoffman, S. C. Wei, A. P. Cogdill, L. Zhao, C. W. Hudgens, D. S. Hutchinson, T. Manzo, M. Petaccia de Macedo, T. Cotechini, T. Kumar, W. S. Chen, S. M. Reddy, R. Szczepaniak Sloane, J. Galloway-Pena, H. Jiang, P. L. Chen, E. J. Shpall, K. Rezvani, A. M. Alousi, R. F. Chemaly, S. Shelburne, L. M. Vence, P. C. Okhuysen, V. B. Jensen, A. G. Swennes, F. McAllister, E. Marcelo Riquelme Sanchez, Y. Zhang, E. Le Chatelier, L. Zitzvogel, N. Pons, J. L. Austin-Breneman, L. E. Haydu, E. M. Burton, J. M. Gardner, E. Sirmans, J. Hu, A. J. Lazar, T. Tsujikawa, A. Diab, H. Tawbi, I. C. Glitza, W. J. Hwu, S. P. Patel, S. E. Woodman, R. N. Amaria, M. A. Davies, J. E. Gershenwald, P. Hwu, J. E. Lee, J. Zhang, L. M. Coussens, Z. A. Cooper, P. A. Futreal, C. R. Daniel, N. J. Ajami, J. F. Petrosino, M. T. Tetzlaff, P. Sharma, J. P. Allison, R. R. Jenq, J. A. Wargo, Gut microbiome modulates response to anti-PD-1 immunotherapy in melanoma patients. *Science* **359**, 97–103 (2018).
24. B. D. Wallace, H. Wang, K. T. Lane, J. E. Scott, J. Orans, J. S. Koo, M. Venkatesh, C. Jobin, L.-A. Yeh, S. Mani, M. R. Redinbo, Alleviating cancer drug toxicity by inhibiting a bacterial enzyme. *Science* **330**, 831–835 (2010).
25. T. A. Suzuki, J. L. Fitzstevens, V. T. Schmidt, H. Enav, K. E. Huus, M. Mbong Ngwese, A. Grießhammer, A. Pfleiderer, B. R. Adegbite, J. F. Zinsou, M. Esen, T. P. Velavan, A. A. Adegnika, L. H. Song, T. D. Spector, A. L. Muehlbauer, N. Marchi, H. Kang, L. Maier, R. Blekhman, L. Ségurel, G. Ko, N. D. Youngblut, P. Kremsner, R. E. Ley, Codiversification of gut microbiota with humans. *Science* **377**, 1328–1332 (2022).
26. K. A. Lee, A. M. Thomas, L. A. Bolte, J. R. Björk, L. K. de Ruijter, F. Armanini, F. Asnicar, A. Blanco-Miguez, R. Board, N. Calbet-Llopard, L. Derosa, N. Dhomen, K. Brooks, M. Harland, M. Harries, E. R. Leeming, P. Lorigan, P. Manghi, R. Marais, J. Newton-Bishop, L. Nezi, F. Pinto, M. Potrony, S. Puig, P. Serra-Bellver, H. M. Shaw, S. Tamburini, S. Valpione, A. Vijay, L. Waldron, L. Zitzvogel, M. Zolfo, E. G. E. de Vries, P. Nathan, R. S. N. Fehrmann, V. Bataille, G. A. P. Hospers, T. D. Spector, R. K. Weersma, N. Segata, Cross-cohort gut microbiome associations with immune checkpoint inhibitor response in advanced melanoma. *Nat. Med.* **28**, 535–544 (2022).
27. D. Shalon, R. N. Culver, J. A. Grembi, J. Folz, P. V. Treit, H. Shi, F. A. Rosenberger, L. Dethlefsen, X. Meng, E. Yaffe, A. Aranda-Díaz, P. E. Geyer, J. B. Mueller-Reif, S. Spencer, A. D. Patterson, G. Triadafilopoulos, S. P. Holmes, M. Mann, O. Fiehn, D. A. Relman, K. C. Huang, Profiling the human intestinal environment under physiological conditions. *Nature* **617**, 581–591 (2023).
28. G. Wang, S. Menon, L. Wilsack, R. Rehak, L. Lou, C. Turbide, J. Auger, A. Tremblay, O. Mathieu, S. Binda, T. A. Tompkins, S. Bruehlmann, C. N. Andrews, Spatially and temporally precise microbiome profiling in the small intestine using the SIMBA capsule with X-ray tracking. *Front.*

Microbiomes **3** (2024), doi:10.3389/frmbi.2024.1321624.

29. Y. Kawasaki, K. Kakimoto, Y. Tanaka, H. Shimizu, K. Nishida, K. Numa, N. Kinoshita, Y. Tatsumi, K. Nakazawa, R. Koshiba, Y. Hirata, K. Ota, N. Sakiyama, T. Terazawa, T. Takeuchi, T. Miyazaki, M. Goto, H. Yokota, Y. Makizaki, Y. Tanaka, S. Nakajima, H. Ohno, K. Higuchi, S. Nakamura, H. Nishikawa, Relationship between Chemotherapy-Induced Diarrhea and Intestinal Microbiome Composition. *Digestion* **104**, 357–369 (2023).
30. Y. Gao, P. Xu, D. Sun, Y. Jiang, X.-L. Lin, T. Han, J. Yu, C. Sheng, H. Chen, J. Hong, Y. Chen, X.-Y. Xiao, J.-Y. Fang, *Faecalibacterium prausnitzii* Abrogates Intestinal Toxicity and Promotes Tumor Immunity to Increase the Efficacy of Dual CTLA4 and PD-1 Checkpoint Blockade. *Cancer Res.* **83**, 3710–3725 (2023).
31. A. Gunjur, Y. Shao, T. Rozday, O. Klein, A. Mu, B. W. Haak, B. Markman, D. Kee, M. S. Carlino, C. Underhill, S. Frentzas, M. Michael, B. Gao, J. Palmer, J. Cebon, A. Behren, D. J. Adams, T. D. Lawley, A gut microbial signature for combination immune checkpoint blockade across cancer types. *Nat. Med.* **30**, 797–809 (2024).
32. V. G. Lewis, M. P. Ween, C. A. McDevitt, The role of ATP-binding cassette transporters in bacterial pathogenicity. *Protoplasma* **249**, 919–942 (2012).
33. J. Jovel, A. Nimaga, T. Jordan, S. O’Keefe, J. Patterson, A. Thiesen, N. Hotte, M. Bording-Jorgensen, S. Subedi, J. Hamilton, E. J. Carpenter, B. Lauga, S. Elahi, K. L. Madsen, G. K.-S. Wong, A. L. Mason, Metagenomics Versus Metatranscriptomics of the Murine Gut Microbiome for Assessing Microbial Metabolism During Inflammation. *Front. Microbiol.* **13**, 829378 (2022).
34. H. Imai, K. Saijo, K. Komine, Y. Yoshida, K. Sasaki, A. Suzuki, K. Ouchi, M. Takahashi, S. Takahashi, H. Shirota, M. Takahashi, C. Ishioka, Antibiotics Improve the Treatment Efficacy of Oxaliplatin-Based but Not Irinotecan-Based Therapy in Advanced Colorectal Cancer Patients. *J. Oncol.* **1**, 1701326 (2020).
35. K. Takasuna, T. Hagiwara, M. Hirohashi, M. Kato, M. Nomura, E. Nagai, T. Yokoi, T. Kamataki, Inhibition of intestinal microflora beta-glucuronidase modifies the distribution of the active metabolite of the antitumor agent, irinotecan hydrochloride (CPT-11) in rats. *Cancer Chemother. Pharmacol.* **42**, 280–286 (1998).
36. D. Flieger, C. Klassert, S. Hainke, R. Keller, R. Kleinschmidt, W. Fischbach, Phase II clinical trial for prevention of delayed diarrhea with cholestyramine/levofloxacin in the second-line treatment with irinotecan biweekly in patients with metastatic colorectal carcinoma. *Oncology* **72**, 10–16 (2007).
37. R.-H. Xu, K. Muro, S. Morita, S. Iwasa, S. W. Han, W. Wang, M. Kotaka, M. Nakamura, J. B. Ahn, Y.-H. Deng, T. Kato, S.-H. Cho, Y. Ba, H. Matsuoka, K.-W. Lee, T. Zhang, Y. Yamada, J.

- Sakamoto, Y. S. Park, T. W. Kim, Modified XELIRI (capecitabine plus irinotecan) versus FOLFIRI (leucovorin, fluorouracil, and irinotecan), both either with or without bevacizumab, as second-line therapy for metastatic colorectal cancer (AXEPT): a multicentre, open-label, randomised, non-inferiority, phase 3 trial. *Lancet Oncol.* **19**, 660–671 (2018).
38. W. H. Gmeiner, A narrative review of genetic factors affecting fluoropyrimidine toxicity. *Precis Cancer Med* **4** (2021), doi:10.21037/pcm-21-17.
39. J. A. Seltzer, N. A. Friedman, J. Hardin, H. Galust, F. L. Cantrell, A. Minns, Oral Capecitabine Exposures and Use of Uridine Triacetate: A 20-Year Retrospective Analysis. *Clin. Drug Investig.* **43**, 359–363 (2023).
40. C.-W. Chang, H.-C. Lee, L.-H. Li, J.-S. Chiang Chiau, T.-E. Wang, W.-H. Chuang, M.-J. Chen, H.-Y. Wang, S.-C. Shih, C.-Y. Liu, T.-H. Tsai, Y.-J. Chen, Fecal Microbiota Transplantation Prevents Intestinal Injury, Upregulation of Toll-Like Receptors, and 5-Fluorouracil/Oxaliplatin-Induced Toxicity in Colorectal Cancer. *Int. J. Mol. Sci.* **21** (2020), doi:10.3390/ijms21020386.
41. P. Osterlund, T. Ruotsalainen, R. Korpela, M. Saxelin, A. Ollus, P. Valta, M. Kouri, I. Elomaa, H. Joensuu, Lactobacillus supplementation for diarrhoea related to chemotherapy of colorectal cancer: a randomised study. *Br. J. Cancer* **97**, 1028–1034 (2007).
42. A. D. Wagner, A. Grothey, T. Andre, J. G. Dixon, N. Wolmark, D. G. Haller, C. J. Allegra, A. de Gramont, E. VanCutsem, S. R. Alberts, T. J. George, M. J. O'Connell, C. Twelves, J. Taieb, L. B. Saltz, C. D. Blanke, E. Francini, R. Kerr, G. Yothers, J. F. Seitz, S. Marsoni, R. M. Goldberg, Q. Shi, Sex and adverse events of adjuvant chemotherapy in colon cancer: An analysis of 34 640 patients in the ACCENT database. *J. Natl. Cancer Inst.* **113**, 400–407 (2021).
43. H. Zeng, H. Yu, L. Lu, D. Jain, M. S. Kidd, M. W. Saif, S. J. Chanock, P. Hartge, PanScan Consortium, H. A. Risch, Genetic effects and modifiers of radiotherapy and chemotherapy on survival in pancreatic cancer. *Pancreas* **40**, 657–663 (2011).
44. A. B. Van Kuilenburg, P. Vreken, N. G. Abeling, H. D. Bakker, R. Meinsma, H. Van Lenthe, R. A. De Abreu, J. A. Smeitink, H. Kayserili, M. Y. Apak, E. Christensen, I. Holopainen, K. Pulkki, D. Riva, G. Botteon, E. Holme, M. Tulinius, W. J. Kleijer, F. A. Beemer, M. Duran, K. E. Niezen-Koning, G. P. Smit, C. Jakobs, L. M. Smit, A. H. Van Gennip, Genotype and phenotype in patients with dihydropyrimidine dehydrogenase deficiency. *Hum. Genet.* **104**, 1–9 (1999).
45. J. E. Knikman, M. Lopez-Yurda, D. Meulendijks, M. J. Deenen, J. H. M. Schellens, J. Beijnen, A. Cats, H.-J. Guchelaar, A Nomogram to Predict Severe Toxicity in DPYD Wild-Type Patients Treated With Capecitabine-Based Anticancer Regimens. *Clin. Pharmacol. Ther.* **115**, 269–277 (2024).
46. C. Palles, S. Fotheringham, L. Chegwidden, M. Lucas, R. Kerr, G. Mozolowski, D. Rosmarin, J. C.

- Taylor, I. Tomlinson, D. Kerr, An Evaluation of the Diagnostic Accuracy of a Panel of Variants in DPYD and a Single Variant in ENOSF1 for Predicting Common Capecitabine Related Toxicities. *Cancers* **13**, 1497 (2021).
47. I. R. Judson, P. J. Beale, J. M. Trigo, W. Aherne, T. Crompton, D. Jones, E. Bush, B. Reigner, A human capecitabine excretion balance and pharmacokinetic study after administration of a single oral dose of 14C-labelled drug. *Invest. New Drugs* **17**, 49–56 (1999).
48. B. Reigner, K. Blesch, E. Weidekamm, Clinical Pharmacokinetics of Capecitabine. *Clin. Pharmacokinet.* **40**, 85–104 (2001).
49. B. Reigner, S. Clive, J. Cassidy, D. Jodrell, R. Schulz, T. Goggin, L. Banken, B. Roos, M. Utoh, T. Mulligan, E. Weidekamm, Influence of the antacid Maalox on the pharmacokinetics of capecitabine in cancer patients. *Cancer Chemother. Pharmacol.* **43**, 309–315 (1999).
50. A. T. Nies, T. Magdy, M. Schwab, U. M. Zanger, J. D. Schuetz, T. Ishikawa, Eds. Role of ABC transporters in fluoropyrimidine-based chemotherapy response. *Adv. Cancer Res.* **125**, 217–243 (2015).
51. H. T. B. Ho, J. Wang, in *Drug Transporters: Molecular Characterization and Role in Drug Disposition*, G. You, M. E. Morrise, Eds. (John Wiley & Sons, Inc., Hoboken, NJ, 2014), pp. 107–126.
52. M. Pastor-Anglada, S. Pérez-Torras, Emerging Roles of Nucleoside Transporters. *Front. Pharmacol.* **9**, 606 (2018).
53. M. Pastor-Anglada, F. J. Casado, in *Deoxynucleoside Analogs In Cancer Therapy*, Cancer Drug Discovery and Development. G. D. Peters, Ed. (Humana Press, 2006), pp. 1–28.
54. L. Timmers, C. C. L. M. Boons, D. Mangnus, P. M. Van de Ven, P. H. Van den Berg, A. Beeker, E. L. Swart, R. J. Honeywell, G. J. Peters, E. Boven, J. G. Hugtenburg, Adherence and Patients' Experiences with the Use of Capecitabine in Daily Practice. *Front. Pharmacol.* **7**, 310 (2016).
55. H. Shindoh, K. Nakano, T. Yoshida, M. Ishigai, Comparison of in vitro metabolic conversion of capecitabine to 5-FU in rats, mice, monkeys and humans--toxicological implications. *J. Toxicol. Sci.* **36**, 411–422 (2011).
56. K. Ota, T. Takeuchi, Y. Kojima, S. Harada, H. Ozaki, N. Sugawara, Y. Hirata, T. Yamaguchi, T. Terazawa, K. Kakimoto, T. Kii, M. Goto, K. Higuchi, Fluoropyrimidine-induced intestinal mucosal injury is associated with the severity of chemotherapy-related diarrhea. *Scand. J. Gastroenterol.* **54**, 227–232 (2019).
57. E. Van Cutsem, P. M. Hoff, P. Harper, R. M. Bukowski, D. Cunningham, P. Dufour, U. Graeven, J. Lokich, S. Madajewicz, J. A. Maroun, J. L. Marshall, E. P. Mitchell, G. Perez-Manga, P. Rougier, W. Schmiegel, J. Schoelmerich, A. Sobrero, R. L. Schilsky, Oral capecitabine vs intravenous 5-

- fluorouracil and leucovorin: integrated efficacy data and novel analyses from two large, randomised, phase III trials. *Br. J. Cancer* **90**, 1190–1197 (2004).
58. M. Hall, R. G. Beiko, in *Microbiome Analysis: Methods and Protocols*, Methods in Molecular Biology. R. G. Beiko, W. Hsiao, J. Parkinson, Eds. (Springer New York, New York, NY, 2018), vol. 1849, pp. 113–129.
59. C. Quast, E. Pruesse, P. Yilmaz, J. Gerken, T. Schweer, P. Yarza, J. Peplies, F. O. Glöckner, The SILVA ribosomal RNA gene database project: improved data processing and web-based tools. *Nucleic Acids Res.* **41**, D590-6 (2013).
60. S. Chen, Y. Zhou, Y. Chen, J. Gu, fastp: an ultra-fast all-in-one FASTQ preprocessor. *Bioinformatics* **34**, i884–i890 (2018).
61. K. Rotmistrovsky, R. Agarwala, *BMTagger: Best Match Tagger for removing human reads from metagenomics datasets* (National Institutes of Health, 2011).
62. A. Blanco-Míguez, F. Beghini, F. Cumbo, L. J. McIver, K. N. Thompson, M. Zolfo, P. Manghi, L. Dubois, K. D. Huang, A. M. Thomas, W. A. Nickols, G. Piccinno, E. Piperni, M. Punčochář, M. Valles-Colomer, A. Tett, F. Giordano, R. Davies, J. Wolf, S. E. Berry, T. D. Spector, E. A. Franzosa, E. Pasolli, F. Asnicar, C. Huttenhower, N. Segata, Extending and improving metagenomic taxonomic profiling with uncharacterized species using MetaPhlAn 4. *Nat. Biotechnol.* **41**, 1633–1644 (2023).
63. F. Beghini, L. J. McIver, A. Blanco-Míguez, L. Dubois, F. Asnicar, S. Maharjan, A. Mailyan, P. Manghi, M. Scholz, A. M. Thomas, M. Valles-Colomer, G. Weingart, Y. Zhang, M. Zolfo, C. Huttenhower, E. A. Franzosa, N. Segata, Integrating taxonomic, functional, and strain-level profiling of diverse microbial communities with bioBakery 3. *eLife* **10** (2021), doi:10.7554/eLife.65088.
64. S. Nayfach, K. S. Pollard, Average genome size estimation improves comparative metagenomics and sheds light on the functional ecology of the human microbiome. *Genome Biol.* **16**, 51 (2015).
65. P. J. McMurdie, S. Holmes, phyloseq: an R package for reproducible interactive analysis and graphics of microbiome census data. *PLoS One* **8**, e61217 (2013).
66. P. Dixon, VEGAN, a package of R functions for community ecology. *J. Veg. Sci.* **14**, 927–930 (2003).
67. J. Pinheiro, D. Bates, S. Debroy, D. Sarkar, R. C. Team, Others, Nlme: nonlinear mixed-effects models. *R package* **3** (2013) (available at <https://docs.w3cub.com/r/library/nlme/html/nlme>).
68. G. Yu, L.-G. Wang, Y. Han, Q.-Y. He, clusterProfiler: an R package for comparing biological themes among gene clusters. *OMICS* **16**, 284–287 (2012).
69. R. Ihaka, R. Gentleman, R: A Language for Data Analysis and Graphics. *J. Comput. Graph. Stat.* **5**, 299–314 (1996).

70. L. Wilkinson, *ggplot2: Elegant Graphics for Data Analysis* by WICKHAM, H. *Biometrics* **67**, 678–679 (2011).
71. A. Kassambara, *Ggpubr: “ggplot2” based publication ready plots* (2018).
72. X. Robin, N. Turck, A. Hainard, N. Tiberti, F. Lisacek, J.-C. Sanchez, M. Müller, *pROC: an open-source package for R and S+ to analyze and compare ROC curves*. *BMC Bioinformatics* **12**, 77 (2011).
73. N. Fidelman, C. E. Atreya, M. Griffith, M. A. Milloy, J. Carnevale, P. Cinar, A. P. Venook, K. Van Loon, Phase I prospective trial of TAS-102 (trifluridine and tipiracil) and radioembolization with 90Y resin microspheres for chemo-refractory colorectal liver metastases. *BMC Cancer* **22**, 1307 (2022).
74. B. J. Callahan, P. J. McMurdie, M. J. Rosen, A. W. Han, A. J. A. Johnson, S. P. Holmes, *DADA2: High-resolution sample inference from Illumina amplicon data*. *Nat. Methods* **13**, 581–583 (2016).
75. S. Fleige, V. Walf, S. Huch, C. Prgomet, J. Sehm, M. W. Pfaffl, Comparison of relative mRNA quantification models and the impact of RNA integrity in quantitative real-time RT-PCR. *Biotechnol. Lett.* **28**, 1601–1613 (2006).
76. J. H. Theil, J. Ahloy-Dallaire, E. M. Weber, B. N. Gaskill, K. R. Pritchett-Corning, S. A. Felt, J. P. Garner, The epidemiology of fighting in group-housed laboratory mice. *Sci. Rep.* **10**, 16649 (2020).
77. D. Cao, A. Ziembka, J. McCabe, R. Yan, L. Wan, B. Kim, M. Gach, S. Flynn, G. Pizzorno, Differential expression of uridine phosphorylase in tumors contributes to an improved fluoropyrimidine therapeutic activity. *Mol. Cancer Ther.* **10**, 2330–2339 (2011).
78. C. Monneret, Platinum anticancer drugs. From serendipity to rational design. *Ann. Pharm. Fr.* **69**, 286–295 (2011).
79. M. Upadhyay, S. K. R. Adena, H. Vardhan, S. K. Yadav, B. Mishra, Locust bean gum and sodium alginate based interpenetrating polymeric network microbeads encapsulating Capecitabine: Improved pharmacokinetics, cytotoxicity & in vivo antitumor activity. *Mater. Sci. Eng. C Mater. Biol. Appl.* **104**, 109958 (2019).
80. *TEVA-CAPECITABINE Product Monograph* (Teva Standard, 2020; https://pdf.hres.ca/dpd_pm/00057941.PDF).
81. A. Loganayagam, M. Arenas Hernandez, A. Corrigan, L. Fairbanks, C. M. Lewis, P. Harper, N. Maisey, P. Ross, J. D. Sanderson, A. M. Marinaki, Pharmacogenetic variants in the DPYD, TYMS, CDA and MTHFR genes are clinically significant predictors of fluoropyrimidine toxicity. *Br. J. Cancer* **108**, 2505–2515 (2013).

82. N. Urbelienė, M. Tiškus, G. Tamulaitienė, R. Gasparavičiūtė, R. Lapinskaitė, V. Jauniškis, J. Sūdžius, R. Meškienė, D. Tauraitė, E. Skrodenytė, G. Urbelis, J. Vaitekūnas, R. Meškys, Cytidine deaminases catalyze the conversion of N(S,O)4-substituted pyrimidine nucleosides. *Sci. Adv.* **9**, eade4361 (2023).
83. Y. Tang, M. Ni, W. Wu, J. Sun, C. Zhou, Biotransformation of the antitumor intermediate 5-fluorouridine by recombinant Escherichia coli with high pyrimidine nucleoside phosphorylase activity. *Biocatal. Biotransformation* **28**, 130–136 (2010).
84. E. Hishinuma, E. Gutiérrez Rico, M. Hiratsuka, In vitro assessment of fluoropyrimidine-metabolizing enzymes: Dihydropyrimidine dehydrogenase, dihydropyrimidinase, and β-ureidopropionase. *J. Clin. Med. Res.* **9**, 2342 (2020).
85. I. Gurevic, Z. Islam, K. Świderek, K. Trepka, A. K. Ghosh, V. Moliner, A. Kohen, Experimental and computational studies delineate the role of asparagine 177 in hydride transfer for *E. coli* thymidylate synthase. *ACS Catal.* **8**, 10241–10253 (2018).
86. M. Burghard-Schrod, S. Altenburger, P. L. Graumann, The *Bacillus subtilis* dCMP deaminase ComEB acts as a dynamic polar localization factor for ComGA within the competence machinery. *Mol. Microbiol.* **113**, 906–922 (2020).
87. D. B. Longley, D. P. Harkin, P. G. Johnston, 5-fluorouracil: mechanisms of action and clinical strategies. *Nat. Rev. Cancer* **3**, 330–338 (2003).
88. B. Rosener, thesis, UMass Chan Medical School (2023).
89. V. Singh, M. Brecik, R. Mukherjee, J. C. Evans, Z. Svetlíková, J. Blaško, S. Surade, J. Blackburn, D. F. Warner, K. Mikušová, V. Mizrahi, The complex mechanism of antimycobacterial action of 5-fluorouracil. *Chem. Biol.* **22**, 63–75 (2015).
90. K. Ghoshal, S. T. Jacob, An alternative molecular mechanism of action of 5-fluorouracil, a potent anticancer drug. *Biochem. Pharmacol.* **53**, 1569–1575 (1997).